Be-10 exposure dating of the timing of Neoglacial glacier advances in the Ecrins-Pelvoux massif, southern French Alps

Melaine Le Roy, Philip Deline, Julien Carcaillet, Irene Schimmelpfennig, Magali Ermini, Georges Aumaitre, D.L. Bourles, Karim Keddadouche

Highlights

- A new TCN-based Neoglacial glacier record for the western European Alps.
- At least five LIA-like advances occurred during the last 4200 years.
- Direct dating of a prominent glacier advance coeval with the 4.2 ka event
- Other LIA-like advances occurred 3.7 ka, 2.1 ka, 1.3 ka and 0.9 ka ago
- We review NH evidence for glacier advance related to the 4.2 ka event

^{10}Be exposure dating of the timing of Neoglacial glacier advances in the Ecrins-Pelvoux massif, southern French Alps

Melaine Le Roy [a], Philip Deline [a], Julien Carcaillet [b], Irene Schimmelpfennig [c], Magali Ermini [c] and ASTER Team [c] *

[a] EDYTEM, Université Savoie Mont Blanc, CNRS, Le Bourget du Lac, France
[b] ISTerre, Université Grenoble Alpes, CNRS, Grenoble, France
[c] CEREGE, Aix-Marseille Université, CNRS, IRD, Coll. France, Aix-en-Provence, France
* Georges Aumaître, Didier L. Bourlès and Karim Keddadouche

Abstract

Alpine glacier variations are known to be reliable proxies of Holocene climate. Here, we present a terrestrial cosmogenic nuclide (TCN)-based glacier chronology relying on 24 new ^{10}Be exposure ages, which constrain maximum Neoglacial positions of four small to mid-sized glaciers (Rateau, Lautaret, Bonnepierre and Etages) in the Ecrins-Pelvoux Massif, southern French Alps. Glacier advances, marked by (mainly lateral) moraine ridges that are located slightly outboard of the Little Ice Age (LIA, c. 1250-1860 AD) maximum positions, were dated to 4.25 ± 0.44 ka, 3.66 ± 0.09 ka, 2.09 ± 0.10 ka, c. 1.31 ± 0.17 ka and to 0.92 ± 0.02 ka. The '4.2 ka advance', albeit constrained by rather scattered dates, is to our knowledge exposure-dated here for the first time in the Alps. It is considered as one of the first major Neoglacial advance in the western Alps, in agreement with other regional paleoclimatological proxies. We further review Alpine and Northern Hemisphere mid-to-high latitude evidence for climate change and glacier activity concomitant with the '4.2 ka event'. The '2.1 ka advance' was not extensively dated in the Alps and is thought to represent a prominent advance in early Roman times. Other Neoglacial advances dated here match the timing of previously described Alpine Neoglacial events. Our results also suggest that a Neoglacial maximum occurred at Etages Glacier 0.9 ka ago, i.e. during the Medieval Climate Anomaly (MCA, c. 850-1250 AD). At Rateau Glacier, discordant results are thought to reflect exhumation and snow cover of the shortest moraine boulders. Overall, this study highlights the need to combine several sites to develop robust Neoglacial glacier chronologies in order to

take into account the variability in moraine deposition pattern and landform obliteration and conservation.

Keywords: Holocene, Neoglacial, Glacier chronology, 4.2 ka event, TCN dating, ^{10}Be, southern French Alps

1. Introduction

The considerable quasi-global glacial wastage that has been taking place for more than a century is currently accelerating in the European Alps (**Vincent et al., 2017**) in response to a warming trend that is higher than the hemispheric average (**Auer et al., 2007**). Glacier mass changes measured over the last three decades cannot be explained without accounting for anthropogenic forcing (**Marzeion et al., 2014**). Conversely, glacier mass losses immediately following the end of the Little Ice Age appear to have been primarily driven by natural forcings (**Vincent et al., 2005**; **Lüthi, 2014**; **Marzeion et al., 2014**; **Sigl et al., 2016**). The knowledge of the timing and amplitude of Holocene LIA-type glacial events and the underlying natural climate forcings could improve our understanding of the glacier evolution and responsible climate drivers since the LIA. Though, the temporal and spatial patterns of such glacial events remain poorly constrained, making causes highly debated (**Wanner et al., 2011**; **Solomina et al., 2015**; **2016**). A better spatio-temporal knowledge of Holocene climate characteristics is necessary to decipher forcing factors and improve climate model simulations (**Schmidt et al., 2014**; **McCaroll, 2015**).

Small to medium-sized alpine glaciers react sensitively to short-term climate variations (**Jóhannesson et al., 1989**; **Oerlemans, 2005**; **Six and Vincent, 2014**; **Roe et al., 2017**). This has last been evidenced in the Alps by the decadal-scale period of minor climate deterioration in the second half of the 20th century that led to significant glacier advances and moraine deposition in the early 1980s (**Patzelt, 1985**). The glacial-geologic record (i.e. moraine ridge stratigraphy) is hence often considered as one of the most straightforward climate proxies beyond the instrumental period (e.g. **Putnam et al., 2012**; **Young et al., 2015**). However, full use of this archive as paleoclimate proxy is restricted by its discontinuous nature, by the selective preservation of glacial deposits and by possible non-climatic controls on moraine

deposition, such as glacier stagnation or advance due to coverage of the glacier tongue by rockfall debris.

The glacial geologic record could differ between nearby sites due to different glacier hypsometry and ice-flow dynamics (**Winkler et al., 2010**; **Barr and Lowell, 2014**). For this reason, dating of moraine complexes provides not only insights into the timing of past glacier-friendly periods, but also allows interpreting the glacial record in terms of landform deposition, conservation and obliteration (**Gibbons et al., 1984**; **Kirkbride and Winkler, 2012**; **Barr and Lowell, 2014**). Well-distributed regionally-significant chronologies based on a homogeneous set of glaciers (size, hypsometry) are therefore requisite to obtain a more complete picture of glacier advances in response to local climate changes. This is particularly true with regard to the Neoglacial, a period during which the glacier advances were of nearly the same magnitude throughout the Northern Hemisphere (**Solomina et al., 2015**), favouring self-censoring of the moraine record. These chronologies will also permit to assess if climate was the main driver of the glacier variations, because non-climatic controls should not affect several glaciers simultaneously.

There is still a dramatic lack of direct constraints on Holocene glacier variability in the westernmost Alps. Investigations on the French side of the Alps have mainly focused on the Mont Blanc massif (see **Le Roy et al., 2015** and references therein). The Ecrins-Pelvoux massif (hereafter EPM) is the south-westernmost currently glaciated area in the European Alps – with the exception of isolated and soon-disappeared glacierets located in the Belledonne massif to the west and in the Ubaye and Maritime Alps massifs to the south (**Fig. 1a**). To deal with the problem of representativeness and selective preservation of moraine deposits we sampled the outermost Holocene ridges at four different glacier forefields located throughout the EPM (**Fig. 1b**). The aim of this study was to obtain a local-scale overview of the timing of Holocene/Neoglacial maxima. We present ^{10}Be exposure ages constraining glacier advances that were almost as extended as the late-LIA stages, marked by the so-called 'AD 1850 moraines'. Given the location of the dated moraine segments, at most a few tens of meters outboard of the LIA extent, we consider in the following text that glacier size during these advances was virtually the same as during the ensuing LIA maxima.

Fig. 1

2. Study area and previous work

The EPM (centred on 44°55'N 6°17'E) belongs to the external crystalline massifs of the western Alps. It consists of blocks of European basement, which was intruded by granites and metamorphosed during the Hercynian orogeny, then exhumed along crustal-scale faults since Oligocene–Early Miocene times. Remnants of inverted Jurassic sedimentary basins are interspersed between these blocks (**Dumont et al., 2008**). Hence, bedrock lithologies of the glaciated catchments are mostly quartz-rich granites and gneisses (**Barbier et al., 1976**; **Barféty and Pêcher, 1984**).

The massif presents a high alpine topography with several summits reaching c. 4000 m a.s.l. (**Fig. 1b**) and valley bottoms around 1000-1500 m a.s.l. Imprint of Quaternary glaciations on present-day landscape is strong as shown by the U-shaped valley profiles, valley rock steps and overdeepenings, lateral hanging valleys, and widespread glacial trimlines (**Montjuvent, 1974**; **Delunel et al., 2010b**; **Valla et al., 2010**). Last Glacial Maximum (LGM) ice cover has been reconstructed from mapping and interpolation of glacial features (**van der Beek and Bourbon, 2008**). Geomorphic evidence also permitted to reconstruct the LIA glacier extent, which amounted to c. 171 km² (**Fig. 1b**; **Edouard, 1978**; **Gardent et al., 2014**). Present day glacierization is characterized by highly fractionated small cirque and slope ice bodies (n = 282; mean surface: 0.24 ± 0.6 km^2), which covered 68.6 km^2 in 2009 (**Fig. 1b**; **Gardent et al., 2014**). Few valley glaciers are still present today, and most of them are debris-covered. The two largest glaciers are the debris-free Girose Glacier (5.1 km², that forms an ice surface of 8.1 km² with the contiguous Mont-de-Lans Glacier) and Glacier Blanc (4.8 km^2) (2009 data; **Fig. 1b**).

The deglacial chronology from the LGM maximum was improved recently in the EPM with TCN ages constraining ice thinning and tongue retreat (**Delunel et al., 2010b**). The Younger Dryas stadial has led to readvances, which were mapped in several catchments (**Edouard, 1978**; **Francou, 1981**; **Coûteaux, 1983a**; **1983b**; **Colas, 2000**; **Di Costanzo and Hofmann, 2016**) and numerically-dated only at one location (**Chenet et al., 2016**). It appears that glacier tongues were restricted to the highest cirques at the beginning of the Holocene (e.g. **Coûteaux, 1983a**). State-of-the-art knowledge on the deglaciation was summarized by **Cossart et al. (2011)** for the eastern part of the EPM. However, no studies have focused on the dating of Holocene/Neoglacial stadials in the EPM up to now. Only LIA and post-LIA advances were dated by palynology (**Tessier et al., 1986**) and lichenometry (**Cossart et al., 2006**; **Le Roy and Deline, 2009**; **Le Roy, 2012**). In addition, it should be noted that subfossil woods were found at two glacier forefields in the EPM: at Chardon Glacier (**Fig. 1b; Vivian,**

1979; Le Roy, unpublished data) where one of the samples yielded a radiocarbon age of 1035-1410 cal. AD (med. prob.: 1245 cal. AD; **Vivian, 1979**), and at Etages Glacier (this work). However, in these studies, the circumstances of sampling are either not accurately known or indicate detrital woods of unknown original location. A firm link with glacier variations has therefore not yet been established at these sites. In any case, these wood remains indicate periods when the treeline was at higher elevation – as the sites of recovery are nowadays devoid of woody vegetation – and mostly composed of *Pinus cembra*, a species which is rare today in the study area (**Coûteaux, 1984**).

Pioneering glaciological studies in the EPM date back to the late 19th century with the first punctual glacier length measurements (**Bonaparte, 1891**; **1892**; **Kilian, 1900**) and were intensified in the 20th century (**Jacob and Flusin, 1905**; **Allix et al., 1927**; **Letréguilly and Reynaud, 1989**; **Reynaud, 1998**; **Reynaud and Vincent, 2000**; **Bonet et al., 2016**). Mass balance is surveyed at Glacier Blanc since AD 2000 with the glaciological method, and was reconstructed for earlier dates based on remote sensing data (**Thibert et al., 2005**; **Rabatel et al., 2008; 2016**). Based on remote sensing of the end-of-summer snowline, average ELA was determined to be 3100 ± 80 m for 11 of the main EPM glaciers during the AD 1984-2010 period, with the lowest values occurring during the year 1984 (2995 ± 60 m) and the highest during the year 2003 (3330 ± 75 m) (**Rabatel et al., 2013**). This can be compared to the average value of 2990 ± 110 m computed over the same time interval for 14 glaciers in the Mont Blanc massif, located 120 km north (**Rabatel et al., 2013; Fig. 1a**). Additionally, **Cossart (2011)** derived an ELA rise of c. 250 m between the LIA (2763 ± 174 m) and present day (AD 2004; 3024 ± 175 m) for 60 of the main EPM glaciers applying an Accumulation Area Ratio (AAR) of 0.67.

Fig. 2.

3. Sample sites

The investigated glacier forefields belong to the Romanche (Rateau and Lautaret Glaciers) and Vénéon (Bonnepierre and Etages Glaciers) catchments (**Fig. 1b**). Characteristics of the study sites are given below and in **Tab. 1**

Tab. 1.

3.1. Rateau Glacier

Rateau Glacier is located in the north face of Rateau (3809 m a.s.l.; **Fig. 2a**). It is becoming a mountain-type glacier as the steep slope body will be soon disconnected from the collapsing debris-covered tongue (**Fig. 2a**). During the LIA maxima, Rateau Glacier was connected to the nearby Meije Glacier, and they had together the lowest frontal position in the EPM (**Fig. 2a**; **Tab. 1**). At least two generations of post-LIA frontal moraines can be identified at c. 2210 and c. 2260 m (**Fig. 2a**), likely deposited during the 1920s and the 1980s. During periods of large Holocene extent, Rateau Glacier fed a small left-hand side marginal lobe, which has built a set of nested lateral ridges (**Fig. 2a**). Eight ridges were mapped on the western part of the lobe, among which the four outer were sampled here (MA-MD; **Fig. 3a**). MD is the most individualized and sharp-crested ridge in the sampled set. The three outermost ridges (MA-MC) features more subdued crests, due to erosion, but also because accretion of material has partially covered pre-existing ridges during advances of same magnitude. Today, the marginal lobe is no longer active and has evolved into rock glacier morphology. Historical length surveys provide information on Rateau Glacier recurrences during the post-LIA retreat. A first advance peaked around AD 1891 (> 13 m), followed by the tongue stagnation until 1894; a second advance began between 1907 and 1911 and culminated around 1921-24 (> 35 m), with the highest frontal progression in 1918-19 (**Allix et al., 1927**).

3.2. Lautaret Glacier

Lautaret Glacier is the largest remnant of formerly connected ice bodies that occupy the ENE-faced cirque located below Grand Doigt (3973 m a.s.l.) and Gaspard Peak (3881 m a.s.l.; **Fig. 2b**). All these glaciers are of mountain-type after the disconnection of the presently debris-covered dead-ice tongue. At least five generations of frontal moraines have been mapped (**Fig. 2b**). Two latero-frontal ridges can be traced down to c. 1940 m and c. 1970 m on the right bank of the stream. Around 2150-2170 m, two sets of ridges were likely deposited between the 1890s and the 1920s. Finally, the youngest moraine at the margin of the stagnant ice tongue dates from the early 1980s (**Fig. 3b**). Additionally, four main vegetated ridges were identified atop of the large left lateral composite moraine, around 2340 m (MA-MD; **Fig. 3b**). The TCN sampling site is located on the distal face of the outermost moraine ridge (MA) where only one suitable boulder was found for analysis (**Fig. 3b**). This outer ridge is cross-cutted by the immediately located inboard ridge MB (**Fig. 3b**). Lautaret Glacier was

rarely surveyed: it was found advancing by 23 m between 1890 and 1891 (**Bonaparte, 1892**), and by c. 4 m between 1919 and 1924 (**Allix et al., 1927**).

3.3. Bonnepierre Glacier

Bonnepierre Glacier is a simple, debris-covered, mainly avalanche-fed, valley glacier occupying a cirque located below the 1000 m-high Dôme des Ecrins (4015 m a.s.l.) NW face (**Fig. 2c**). The right lateral moraine extends over 3.1 km between c. 2880 and 2120 m. This large, composite, single crested moraine subdivides into four well-defined nested ridges around 2550 m. However, erosion of the proximal face of the moraine makes difficult to establish a firm correspondence between the innermost segments (**Fig. 3c**). All the segments (MA-ME) were sampled for TCN (**Fig. 3c**). Another set of lateral ridges – not sampled – has been identified at the same elevation atop of the left lateral moraine (**Fig. 2c**). In frontal position, several ridges are present between 2120 m and 2360 m. Lichenometric surveys carried out on these ridges revealed that the maximum frontal extent was achieved at the end of the LIA (c. AD 1854) and that the youngest frontal moraine was deposited during the early 1940s (**Le Roy and Deline, 2009**; **Le Roy, 2012**). Hummocky terrain in between denotes a rapid demise of a likely already debris-covered tongue after the end of the LIA. Lichen measurements were also performed on the lateral ridges MA, MB and ME (60 to 100 measurements per surface; **Le Roy and Deline, 2009**; **Le Roy, 2012)**. Results obtained are 105 mm, 72 mm and 48 mm (mean of the five largest thalli per surface), respectively (**Le Roy and Deline, 2009**; **Le Roy, 2012**). Post-LIA behaviour of Bonnepierre Glacier shows a rapid retreat between AD 1860 and 1890, which then slowed until 1895 and was followed by a nearly stable front over the 20th century (total retreat since 1895 only amounts to 210 m). Periods of still-stand (1895-1899 and 1967-1977) and small advance (+15 m between 1913 and 1922) show that this glacier nevertheless reacted to the 20th century climate downturns (**Allix et al., 1927**; **Edouard, 1978**). Rock avalanche history of this site includes several undated events evidenced by large deposits on the right bank of the valley (**Fig. 2c**), of which one is interstratified in the upper part of the lateral moraine (**Fig. 4c**), pointing to an occurrence during the last millennium. More recently, the collapse of the Clocher des Ecrins (3801 m a.s.l.) summit zone ($< 1 \times 10^4$ m^3) occurred during the winter 1931-1932 (**Bourgeat, 1990**), and a large rock avalanche ($\sim 3.6 \times 10^5$ m^3) occurred in the Flambeau des Ecrins north face (3000 m a.s.l.) on 19th July 2016.

3.4. Etages Glacier

Etages Glacier is a north-facing valley glacier located in a cirque below Pointe du Vallon des Etages (3564 m a.s.l.) and Tête de l'Etret (3559 m a.s.l.). The tongue is disconnected from the small remaining slope ice bodies (**Fig. 2d**). Six frontal moraine ridges were mapped between 2090 and 2355 m (M1-M6; **Fig. 3d**). Sampling for TCN dating was carried out only on the outermost ridge M1, a c. 2-m-high, clast-supported and boulder-rich, frontal moraine remnant dissected by proglacial streams. All moraines (except M4 and M6) were extensively surveyed to locate and measure the largest lichen thalli per boulder (50 to 150 measurements per surface; **Le Roy and Deline, 2009**; **Le Roy, 2012**). On moraine M1, the mean of the five largest thalli amounts to 88.6 mm, which prevents an estimate of the age of this surface based on available growth curve. Moraine M2 is only preserved on the right side of the valley and lacks suitable boulders whether for lichen measurement or TCN sampling. Lichen data collected on this surface (mean five largest: 52.4 mm) are thus considered minimum values for dating purpose. Frontal moraine M3 (c. 4 m high) is quasi-continuous over the entire width of the valley. Lichen measurements (mean of the five largest: 50.2 mm) indicate a stabilisation between AD 1822 and 1853 depending on the method used (see **Le Roy, 2012**). This indicates a deposition of M3 during the last major advance of the LIA. Moraine M5 is dated between 1919 and 1922 depending on the method (mean of the five largest: 29 mm). This is consistent with the first accurate map of Etages Glacier, established in 1929-1930, which shows the tongue already retreating (c. 40 m upstream) from this moraine. Moraine M6, located 180 m downstream from the 2009 front, has formed in the mid-1980s. Finally, a 1.4-m-long detrital subfossil log was found in the proglacial stream at 2160 m, in fall 2008. The sampling location is 800 m downstream from the current glacier front and immediately downstream from a perennial snow patch located at the foot of the avalanche path originating in the Encoula Pass area (**Fig. 2d** and **3d**).

3.5. Glacier/climate relationships

Although glacier tongues are currently debris-covered at our study sites, the climate sensitivity of investigated glaciers is evidenced by historical moraine deposition and available punctual length variation observations presented in Section 3. They indicate that all glaciers have reacted to the three post-LIA climate downturns. By analogy with alpine glaciers for which continuous length observations exist (**Müller, 1988**; **Letréguilly and Reynaud, 1989**; **Reynaud and Vincent, 2000**; **Hoelzle et al., 2007**) a short reaction time characterizes glacier dynamics at our study sites, likely 10-20 years, Bonnepierre Glacier being the ice mass slowest to react.

4. Methods

4.1. Mapping and Equilibrium Line Altitude (ELA) determination

Geomorphic units were mapped based on recent aerial photographs (2009) and field surveys (**Fig. 2**). ELAs were determined for the four glaciers at two different time steps, the Neoglacial/LIA maximum and the early 1980s, during which glaciers were at equilibrium and deposited stadial moraines. For both stadials, a digital elevation model was generated by drawing contour lines of the paleoglaciers (with 50 m step) according to standard procedure (e.g. **Sissons, 1977**). ELAs computation was made with the toolbox developed for ArcGIS by **Pellitero et al. (2015)** with a contour interval set to 10 m. Two methods were implemented. First, an Accumulation Area Ratio (AAR) of 0.67 – which has been widely used for ELA reconstruction in the Alps (e.g. **Gross et al., 1977**; **Maisch et al., 1999**) – was applied. However, this ratio can be significantly lower for glaciers experiencing strong topographical control and/or extensive debris-cover (e.g. Bonnepierre Glacier), resulting in an underestimation of the ELA altitude. At this latter site, a lower AAR value of 0.40 was used (e.g. **Kulkarni, 1992**; **Scherler et al., 2011**). Second, an Area-Altitude Balance Ratio (AABR) of 1.6 – representative for the Alps (**Rea 2009**; **Pellitero et al., 2015**) – was also used, lowered to 0.9 for the debris-covered Bonnepierre Glacier. Resulting ELAs are reported in **Tab. 1**. The maximum elevation of the lateral moraines (MELM) is also shown for each site.

4.2. ^{10}Be sampling

Sampling took place in 2010 and 2012. All samples were collected from boulders that were embedded in the crest or distal face of moraine ridges. In both locations, boulder exposure age is thought to reflect the age of moraine stabilisation. Indeed, landform degradation observations and modelling have shown that a large boulder embedded on distal face mid-slope is unlikely to have experienced significant exhumation or burial on Holocene-aged moraines (**O'Neal, 2006**; **Putkonen and O'Neal, 2006**; **Putkonen et al., 2008**). Consequently, ^{10}Be ages are interpreted as close minimum ages for the culmination of the glacier advances (**Gosse, 2005**). Ridges were chosen for sampling based on their distal location with regard to the fresh appearing late-LIA deposits. Features indicating substantial exposure time (mature lichen cover, well-developed soil) helped to determine sampling sites.

299 A *Rhizocarpon* sp. local growth curve (**Pech et al., 2003**; **Le Roy and Deline, 2009**) and
300 available lichen dates (**Le Roy, 2012**) were used to confirm that sampled ridges were
301 deposited prior to the second half of the LIA. Rock samples were removed from the upper cm
302 of meter-scale flat boulders with hammer and chisel (**Tab. 2**). Location and elevation of the
303 samples were recorded with a handheld GPS, assuming a vertical and horizontal positional
304 uncertainty of ± 10 m and ± 5 m, respectively (**Tab. 2**). Topographic shielding was estimated
305 in the field through skyline survey using a clinometer (**Tab. 2**).
306
307 **Tab. 2**
308
309 *4.3. ^{10}Be geochemistry and AMS measurement*
310 Samples were crushed and sieved to retain the 200-500 µm size fraction. The subsequent
311 beryllium extraction protocol is adapted from **Brown et al. (1991)** and **Merchel and Herpels**
312 **(1999)** chemical procedures. It was carried out at the ISTerre cosmogenic laboratory in
313 Grenoble. Quartz was isolated through magnetic separation and repeated leaching in a
314 H_2SiF_6-HCl mixture. Meteoric Be purification was achieved with three sequential baths in
315 diluted HF (**Kohl and Nishiizumi, 1992**). The purified quartz samples (between 14 g and 52
316 g) were spiked with ~300 µl of a 1.10^{-3} g g^{-1} Be carrier solution (Scharlab ICP Standard)
317 before being totally dissolved in concentrated HF (**Tab. 3**). After the evaporation of the HF,
318 perchloric and nitric acids were added and evaporated to remove organic compounds and
319 fluorides. Anion and cation exchange columns allowed the separation of Fe and Ti and the
320 isolation of the Be fraction. At last, Be hydroxide was extracted by alkaline precipitation (**von**
321 **Blanckenburg et al., 1996**). The final BeO target were oxidized and mixed with Nb powder
322 prior to loading it on the cathode for AMS measurements, which were carried out at ASTER,
323 the French National AMS facility (CEREGE, Aix-en-Provence; **Arnold et al., 2010**). The
324 measured ^{10}Be/^{9}Be ratios were calibrated against the NIST_27900 beryllium standard
325 Reference Material 4325 by using an assigned value of $2.79 \pm 0.03 \times 10^{-11}$ (**Nishiizumi et al.,**
326 **2007**) and a ^{10}Be half-life of $1.387 \pm 0.012 \times 10^{6}$ years (**Chmeleff et al., 2010**; **Korschinek et**
327 **al., 2010**). The ^{10}Be concentrations inferred from the measured ^{10}Be/^{9}Be ratios are corrected
328 for the corresponding full process blank ratios which range between $(1.4 \pm 0.8) \times 10^{-15}$ and
329 $(9.7 \pm 1.3) \times 10^{-15}$ (n = 7; **Tab. 3**). AMS analytical uncertainties (reported as 1σ) include the
330 uncertainties associated with the AMS counting statistics, with the chemical blank corrections
331 and with the ASTER AMS external error (0.5%; **Arnold et al., 2010**; **Tab. 3**).

Tab. 3

4.4. ^{10}Be age computation

Exposure ages were computed with the online CREp program (**Martin et al., 2017**; http://crep.crpg.cnrs-nancy.fr/#/init; last accessed 06/09/2017) and are presented in **Tab. 3**. Scaling to the sample locations was made according to the recent, physically-based, LSD model (**Lifton et al., 2014**) which performs similarly to older empirical models (**Borchers et al., 2016**). Chosen parameters include the ERA-40 atmosphere model (**Uppala et al., 2005**) and the Lifton VDM 2016 geomagnetic database (**Lifton, 2016**). We retained the production rate (PR) derived by **Claude et al. (2014)** at the Chironico landslide site (Ticino, Switzerland, 260 km NE from the EPM; **Fig. 1a**) which is the only regional PR available so far. This PR has a value of 4.16 ± 0.10 at. g^{-1} yr^{-1} for LSD scaling and is consistent with other recently derived Northern Hemisphere PR (**Balco et al., 2009**; **Fenton et al., 2011**; **Ballantyne and Stone, 2012**; **Briner et al., 2012**; **Goehring et al., 2012**; **Young et al., 2013**; **Small and Fabel, 2015**; **Stroeven et al., 2015)**. In order to make our results easily comparable to previous studies carried in the Alps (e.g. **Schimmelpfennig et al., 2012**; **2014**) we also present in **Tab. 3** exposure ages computed with the CRONUS-Earth online calculator (version 2.2; **Balco et al., 2008**; http://hess.ess.washington.edu/) using the time-dependent 'Lm' scaling model (**Lal, 1991**; **Stone, 2000**), standard atmosphere (**N.O.A.A., 1976**) and the 'Arctic' PR (**Young et al., 2013**) which has a value of 3.93 ± 0.15 at. g^{-1} yr^{-1} for 'Lm' scaling (**Balco et al., 2008**). 'Lm/Arctic' ages are in average only 2.7 % older (80 ± 20 years) than the 'LSD/Chironico' ages used in the discussion hereafter. We therefore stress that the choice of a different PR/scaling model couple would not affect our conclusions. We did not apply erosion- nor snow-corrections given that erosion is negligible for late-Holocene surfaces and that most sampled boulders lie in windswept locations (but see further discussion in Section 5.1). Multiple boulder exposure ages from a single surface (i.e. moraine ridge) were averaged (arithmetic mean) after identification of possible outliers. The uncertainties in the mean ages are represented by the standard deviations of the retained boulders ages plus the production rate uncertainty (2.4 %), added in quadrature. To ensure homogeneity between the different time scale notations used in the discussion and to ease comparisons with dendro-dates and calibrated radiocarbon dates, all exposure ages are hereafter expressed either in ka b2k (before AD 2000) or in calendar years (BC/AD). Radiocarbon dates quoted in the discussion were

recalibrated from original publication using Calib 7.1 (**Stuiver et al., 2017**) and IntCal13 (**Reimer et al., 2013**), and are expressed both by the 2σ interval of calibration and the median of the probability distribution function (**Telford et al., 2004**).

Fig. 3.

5. Results and interpretation

5.1. ELAs determination

Mean ELAs computed for the Neoglacial/LIA maximum are 2737 and 2779 m, depending on the method (**Tab. 1**), which is in good agreement with previous work in the EPM (**Cossart, 2011**). We found a c. 90 m ELA rise (average of the results from both methods) between this stadial and the early 1980s stadial (**Tab. 1**). Without taking into account the nearly stagnant Bonnepierre Glacier, this value amounts to c. 115 m. According to available estimates of ELA climate sensitivity to summer temperature (e.g. **Rabatel et al., 2013**), this value is equivalent to a 0.8 to 1°C warming over the considered period.

5.2. Moraine exposure ages

5.2.1. Rateau Glacier

The nine ages from the four outer moraine ridges (MA, MB, MC and MD) range from c. 2.1 to c. 3.7 ka, a relatively short time span of ~1.6 ka falling within the Late Holocene period. However, the order of these ages clearly disagrees with the moraine ridge stratigraphy, as the four oldest ages are obtained on the inner ridges MC and MD (**Fig. 3a** and **4a**). The entire spread in ages is similar to the one observed on the single innermost sampled ridge MD. Explanations for discordant results in moraine age populations generally include nuclide inheritance from previous exposure durations, exhumation or toppling of some boulders, or seasonal shielding by snow cover (**Schildgen et al., 2005**; **Delunel et al., 2014b**). Here, we consider nuclide inheritance and boulder toppling as unlikely. In the case of nuclide inheritance, a wider and more dispersed spread would be expected in the age population. We retained boulder exhumation, as well as a possible shielding by snow cover of the shortest boulders, as the most probable explanation. This is confirmed by the correlation existing

between the four exposure ages and the heights of the corresponding samples on moraine MD (**Tab. 2 and 3**). Averaging ages from a given ridge is therefore not possible here. Only the tallest boulders are likely to yield a robust estimate for the timing of glacier advance. We therefore tentatively interpret the oldest age on MD (RAT09, sample height above surface: 115 cm) – which is surely the less affected by exhumation and snow cover of all sampled boulders given its geometry – as the best estimate for the deposition of this ridge at 3.66 ka ± 0.45 ka. This implies that the three outermost ridges (MA, MB, and MC) must have been deposited before that date. This interpretation is in accordance with the conclusions of **Heyman et al**. (**2016**) who have demonstrated that the fraction of well-clustered ages on moraine surfaces increases with boulder height cut-off values up to 160 cm. In comparison, mean height of the samples from Rateau Glacier is 0.80 ± 0.24 m (**Tab. 2**). According to this explanation, ages from the ridges MA, MB and MC displayed on **Fig. 3a** must be considered as distant minimum ages and are not taken into account hereafter. As an indication, only apparent ages based on the single oldest age per surface are displayed on **Fig. 4a** for these three outer ridges.

5.2.2. Lautaret Glacier

The unique sample collected at this site from a 110 cm-tall, well-embedded boulder yields an age of 1.31 ka ± 0.17 ka for the outermost lateral ridge MA. Given the size and location of this boulder we consider this is a reliable estimate for the deposition of MA, although it rests on a single age. This gives a maximum age for the three inboard lateral ridges MB-MD that were mapped atop of the left lateral composite moraine (**Fig. 3b** and **4b**).

Fig. 4

5.2.3. Bonnepierre Glacier

The four ages acquired on the outermost ridge MA range from 4.7 to 3.7 ka (**Fig. 3c**). Although there is 1 ka spread within this age population and the oldest (BON03) and the youngest (BON00) ages might be slightly over- and underestimated, respectively, no outlier can be identified based on the Chauvenet's criterion. The mean age of the four boulders is 4.25 ± 0.44 ka, which is in good agreement with the consistent ages of boulders BON02 and BON04 (mean: 4.35 ± 0.11 ka). We therefore consider the average of all four ages a reliable estimate for the timing of deposition of MA (**Fig. 4c**). Given the volume of MA (**Fig. 4c**)

several glacier advances have likely been necessary to build the core of this landform. Only the last advance has been dated here. Ages of these older advances cannot be constrained easily and could date either from the early Holocene or from the Neoglacial before c. 4.3 ka. Finally, the '4.2 ka advance' could possibly have been multi-phased as shown by the presence of a subdued ridge, mid-slope of the distal face of MA (**Fig. 3c**). Anyway, if this has been the case these distinct glacier pulses would have occurred in a very short interval as demonstrated by the similar ages obtained on both the moraine crest (BON02) and at the bottom of the distal face (BON04) (**Fig. 3c**).

The age of the next prominent ridge MB is constrained by two consistent ages (BON05 and BON06; **Fig. 3c**), which give a mean of 3.66 ± 0.10 ka. The small segment MC, which is adjoined to the proximal face of MB (no counter-slope), yields an age of 3.65 ± 0.35 ka based on a single boulder (BON07). This age is indistinguishable from that of MB. We therefore interpret this ridge as having been deposited during the same glacial phase as MB.

Due to erosion, the two innermost segments (MD and ME) don't feature crests. Only part of the distal face is available for sampling (**Fig. 4c**). This resemblance might suggest that both segments would have originally been part of the same ridge. The two boulders sampled on segment MD yield 'too old' ages with respect to the stratigraphy (4.22 ± 0.40 ka for BON12 and 5.63 ± 0.68 ka for BON11; **Fig. 3c**) and were therefore considered as outliers. This inherited component could originate from the deposition of avalanched material pre-exposed in the cirque rock-walls or from the reworking of previously deposited moraine boulders. Since this is a low-level inheritance, leading to Neoglacial ages, we favour here the latter interpretation. On segment ME, boulder BON10 (3.53 ± 0.22 ka) was also considered an outlier as internal uncertainty does not overlap with the other two. Given the similarity of the age of this boulder with the mean age of the immediately outboard located blocky ridges MB/MC, it is likely that this boulder was reworked from the proximal face of MB/MC, before its deposition with the ridge ME (**Fig. 4c**). The two remaining boulders on ME (BON08 and BON09) yield consistent ages and allow proposing a deposition of this ridge at 2.09 ± 0.10 ka, in agreement with the stratigraphy. We have privileged the youngest ages on ME as best estimates of its true deposition age due to morphostratigraphical considerations and to the significantly different lichen data obtained on MB and ME (see Section 3.3), suggesting that these two ridges were not deposited during the same glacial phase. Moreover, based on field observations, it is highly unlikely that these two boulders were exhumed or even toppled after deposition.

Exposure ages acquired at this site show that lichen data (see Section 3.3) are not relevant to estimate the timing of deposition of mid-to-late Holocene moraines in the area. Despite their internal consistency (i.e. conforms to the stratigraphy), lichen measurements available here greatly underestimate moraines ages (see **Le Roy, 2012**). This is likely because of a rejuvenation of the population as the first colonizers are no longer present and saturation of the surfaces occurs. 'Too young' lichen ages were also reported in other settings (e.g. **Wiles et al., 2010**) even if a fair matching between lichenometric and cosmogenic ages could also be noted elsewhere (**Young et al., 2009**) in regions where saturation likely occurs later than in the Alps, due to lower growth rates.

5.2.4. Etages Glacier

Frontal moraine M1 is dated to 0.92 ± 0.02 ka (AD 1085 ± 20) based on the mean of two consistent ages (ETA01 and ETA02; **Fig. 3d**). This date marks the Neoglacial maximum of Etages Glacier.

Independent evidence reinforces the TCN dating of moraine M1 during the MCA. A detrital log (eta01) was found in the proglacial stream below the snow patch, c. 400 m upstream from M1 (**Fig. 3d**). The tree-ring series from this sample was crossdated with two different *Pinus cembra* reference chronology: the Eastern Alpine Conifer Chronology from Tirol (EACC; **Nicolussi et al., 2009**) and a reference from Mont Blanc massif (**Le Roy et al., 2015**). Consistent results indicate this tree lived more than 385 years between AD 632 and 1016+, an unknown number of outer rings being missing due to abrasion (**Fig. 5**). It is not possible to state if the tree death is directly related to glacial activity. This seems however unlikely given the marked eccentric pattern of the tree-rings (**Fig. 5**) – probably resulting from a growth on a steep slope just above the glacier forefield – and the sampling site located directly downstream of a major avalanche path (**Fig. 3d** and **4d**). Nevertheless, its preservation required a fairly rapid burial by glacial sediments. This surely occurred by the end of the 11th century AD (c. 0.9 ka ago), when Etages Glacier likely advanced beyond the location of the avalanche deposit during the course of its Medieval advance.

Fig 5.

Interestingly, a ^{10}Be inventory of glaciogenic material performed by **Delunel et al. (2014a)** in the Etages valley (see **Fig. 3d** for location of their samples) shows good agreement

with our data. They report apparent ages (recalculated here with a ~15 % lower PR) for sand and gravel samples taken at the glacier portal (c. 400 yrs; Rd 59), on the main frontal outwash near moraine M1 (c. 830 and 1410 yrs; Rd 61 and 62), as well as at two locations on the large latero-medial moraine that the authors call 'LIA moraine' (c. 530 and 680 yrs; Rd 60 and 57). Moreover, a zero-concentration was determined for a sample taken from the glacier surface (Rd 58). According to the authors' interpretation, this dataset indicates a significant inherited ^{10}Be component at some locations, because some ages are considered 'too old' for LIA moraines. However, given our results, we consider the latero-medial moraine to be built during part of the Neoglacial, with the two most important advances occurring at c. AD 1100 (deposition of M1) and somewhere between 1100 and the 19th century (deposition of M2). Therefore, ^{10}Be concentrations corresponding to a c. 1 ka-long exposure for samples from the outwash located near moraine M1 are in good agreement with our dating of this ridge at 0.9 ka, as is the early-LIA apparent age determined on the latero-medial moraine (**Fig. 3d**). Finally, the low to null ^{10}Be concentrations measured by **Delunel et al. (2014a)** for the supraglacial load reinforce confidence in ages we obtained on moraine M1, as inheritance seems absent at this site.

5.3. Summary

- The moraines that we were able to date all fall into the Late Holocene period, between c. 4.3 and 0.9 ka (**Fig. 6**).
- The oldest moraine in the data set is dated to 4.3 ± 0.4, which can most likely be correlated with the classical '4.2 ka event' (**Walker et al., 2012**; **Fig. 6**).
- Around 3.7 ka, several moraines were deposited in a short interval at Bonnepierre Glacier and also probably at Rateau Glacier. Other than that, none of the dated moraines is contemporaneous with any one from the other sites. Anyway, because of the close spatial proximity, we consider that the moraines ages are complementary and reflect a common climate signal modulated by respective glacier dynamics.
- The other advances occurred at 2.1 ± 0.1 and likely at 1.3 ± 0.2 ka. The youngest one occurred during the classical MCA at 0.9 ka.
- Exhumation seems to be the main process explaining boulder age discrepancy at Rateau Glacier site, while three boulders showing low-level inheritance were identified on the innermost moraine segments at Bonnepierre Glacier site.

- Mean Neoglacial/LIA ELAs at our studied glaciers were 2737 and 2779 m, depending on the method. We found an ELA rise of c. 90 m (up to c. 115 m excluding Bonnepierre Glacier) between the Neoglacial maxima and the early 1980s.

6. Discussion

6.1. The '4.2 ka advance', one of the first major Neoglacial advance in the Alps

We interpret the '4.2 ka advance' – to our knowledge directly (i.e. exposure-) dated here for the first time in the Alps – as one of the first major Neoglacial advance in this area. Together with data from the literature (Sections 6.1.1, 6.1.2 and 6.2), we propose this advance as possibly marking the onset of this period (**Fig. 6**), defined here as a late-Holocene interval during which prominent advances reached Holocene maxima and no multi-centennial (> 500 yrs) climate optima occurred. This differs from the definition sometimes found, i.e. the renewal of glacial activity (without reaching Holocene maxima on large valley glaciers) following the Holocene Hypsithermal – which starts between c. 6.6 and 5.2 ka, both in the Alps (**Fig. 6c-f**; **Baroni and Orombelli, 1996**; **Orombelli, 1998**; **Nicolussi and Patzelt, 2001**; **Wipf, 2001**; **Deline and Orombelli, 2005**; **Joerin et al., 2008**; **Holzhauser, 2010**; **Nicolussi et al., 2013**; **Gabrielli et al., 2016**) and in northwestern North America (**Menounos et al., 2009**; **Harvey et al., 2012**; **Osborn et al., 2012**; **Luckman et al., 2017**).

Fig 6.

6.1.1. Paleoclimate evidence

There is a wealth of paleoclimatic evidence indicating that the period 4.4–4.0 ka has seen a cooling and an increase in humidity around the north Atlantic. Likewise, this period marks a multi-centennial-scale 'tipping point' in several proxy time-series (**Fig. 6**). North Atlantic lake-sediments records, Alpine treeline variations, and high-elevation speleothems $\delta^{18}O$ records show a marked cooling (**Fig. 6a/b**; **Andresen et al., 2006**; **Fohlmeister et al., 2013**; **Nicolussi et al., 2005**). In central north-western Europe, lake-levels, fluvial geomorphic activity and erosion in the montane zone peaked at that time (**Fig. 6h-j**; **Hoffmann et al., 2008**; **Magny et al., 2011**; **2012a**; **2012b**; **Bajard et al., 2016**), as well as peat humification proxies in oceanic north-western Europe (**Barber et al., 2003**; **Eckstein et al., 2010**). In the

562 southern French Alps, a major detrital pulse centred on 4.2 ka was recorded in a high-
563 elevation catchment (Lake Petit; **Brisset et al., 2013;** see **Fig. 1a** for location). In the same
564 area, a cluster of TCN ages constraining rock avalanches – probably triggered by high rainfall
565 events – appears coeval with this period (**Zerathe et al., 2014**). Close to our study sites, the
566 rock avalanche deposit damming Lauvitel Lake (see **Fig. 1b** for location) was also TCN-dated
567 to this interval, at 4.65 ± 1.3 ka (2650 ± 1300 BC; mean age recalculated here from **Delunel**
568 **et al., 2010a** with four additional ages and without taking into account possible outliers) –
569 which is consistent with the dating of the lake sedimentary fill (**Fouinat et al., 2013**).
570 The most accurate temporal constraint on the '4.2 ka event' is given by a bog-pine dying-
571 off phase which coincides with a major disruption in bog-oak growth indices from 2168 BC
572 onwards in northwest Germany – indicating wet and cool conditions with regional
573 significance (**Eckstein et al., 2010**). Since some other northern Europe bog-tree low-growth
574 and dying-off events – e.g. during the AD 4th and 6th centuries (**Sass-Klaassen and Haenrets,**
575 **2006**) – correspond to known glacier advances in the western Alps (**Holzhauser et al., 2005**;
576 **Le Roy et al., 2015**), this wet/cool c. 4.2 ka period could have triggered positive mass balance
577 in the Alps as well. Cool conditions are confirmed by the $\delta^{18}O$ record of high-elevation
578 speleothems, a proxy for annual temperature, which rose markedly at c. 2165 BC, reaching
579 for the first time since the Preboreal high values that characterize late Holocene cold periods
580 (**Fig. 6a**; **Fohlmeister et al., 2013**). Moreover, dendro-densitometry analyses carried out on
581 timberline subfossil larch trees in the Swiss Alps show an extended drop, reflecting low
582 summer temperature, between 2150 and 2030 BC, with a minimum around 2110 BC
583 (**Renner, 1982**). Our estimate of the age of moraine MA at Bonnepierre Glacier at 4.25 ± 0.44
584 ka (2250 ± 440 BC) thus overlaps with independent evidence for cooling and wetter
585 conditions presented above.
586
587 *6.1.2. Glacier-related evidence*
588 In the Alps, some glaciers were advancing slightly beyond modern positions as early as
589 4.5 ka (**Fig. 6d/f**). In Austrian Alps, an advance of the Schwarzenstein Glacier is recognized
590 after 2870–2500 cal. BC (med. prob.: 2685 cal. BC; **Pindur and Heuberger, 2010**; all cited
591 locations from previous studies are shown in **Fig. 1a**) and the Gepatsch and Pasterze Glaciers
592 reached their AD 1960 and AD 2000 levels, respectively, around 2500 BC (**Nicolussi and**
593 **Patzelt, 2001**). However, in these cases, the maximum extent achieved at that time is not
594 known.

Data relating to the 4.2 ka glacier advance itself are spatially better constrained, as some scarce moraines could tentatively be assigned to this period. At Brenay Glacier (Swiss Alps), a soil buried by the outermost ridge of the Holocene moraine complex has yielded an age of 3485–1965 cal. BC (med. prob.: 2685 cal. BC; **Schneebeli, 1976**). Despite large dating uncertainties, this ridge may have been deposited at the end of the third millennium BC. Similarly, Schmadri Glacier has reached or surpassed its LIA maximum extent after 2460–2040 cal. BC (med. prob.: 2240 cal. BC) as shown by a soil buried below a lateral ridge located 50 m outboard of the LIA maximum moraine (**Wipf, 2001**). Other evidence for contemporary glacier advance without preserved moraine ridges come from Morteratsch Glacier, which slightly exceeded its AD 1862 extent after 2570–2205 cal. BC (med. prob.: 2390 cal. BC) as demonstrated by glacially-sheared *in situ* stumps (**Holzhauser, 2010**). Alike, Rhône Glacier experienced a large advance, slightly exceeding its LIA maximum extent, just after 2570–2135 cal. BC (med. prob.: 2340 cal. BC) as indicated by a reworked buried soil (**Zumbühl and Holzhauser, 1988**; **Holzhauser, 2007**).

At some other sites, the maximum extent of the c. 4.2 ka advance is not precisely known but evidence was found that this cool/wet event represented the end of a long lasting climate optimum. Unambiguous, glacier-related, evidence for this warm period comes as continuous peat growth under the location of the current tongue of Pasterze Glacier (Austrian Alps) between 3360–3100 cal. BC (med. prob.: 3210 cal. BC) and 2460–2210 (med. prob.: 2330 cal. BC). To allow peat colonization, the glacier had to be significantly smaller than its AD 2007 extent during this c. 1 ka interval (**Kellerer-Pirklbauer and Drescher-Schneider, 2009**). In the Italian Alps, radiocarbon-dating of the last rings of a subfossil log found in the Forni Glacier forefield indicates its tongue likely exceeded its AD 1960 level after 2251–2082 cal. BC (med. prob.: 2186 cal. BC), ending a retreat upstream of this position that lasted at least 300 years (**Pelfini et al., 2014**). On the Tisenjoch Pass – the site where Ötzi was discovered – the youngest buried soil was dated to 2560–2150 cal. BC (med. prob.: 2360 cal. BC). It testifies a thinning of the Niederjoch Glacier accumulation area leading to a significant ice-free period at this high-elevation crest site (3215 m a.s.l.) during the third millennium BC (**Baroni and Orombelli, 1996**). In the Swiss Alps, Gauli Glacier exceeded its AD 1980 level for the first time in 400 years after 2835–2155 cal. BC (med. prob.: 2445 cal. BC; **Wäspi, 1993**). Similarly, the slow reacting Gorner Glacier exceeded its AD 1963 level (or a more upstream location) slightly after 2231 BC, as shown by dendro-dating of detrital logs whose outermost rings are lacking. This advance ended a glacier extent similar or shorter than today that lasted at least 650 years at this site (**Holzhauser, 2010**). The Subboreal

629 Climate Optimum (c. 3200–2200 BC) is also particularly visible in the dataset of radiocarbon-
630 dated archeological artefacts from Schnidejoch Pass (**Fig. 7b**; **Hafner and Schwörer, 2017**).
631 The subsequent marked drop of the summed probability density functions (PDFs) of the
632 calibrated radiocarbon ages centred on 2300-2200 BC (**Fig. 7b**) likely indicates an
633 enlargement of the adjoining Chilchli Glacier leading to unfavourable conditions to cross the
634 pass during this interval.
635 South of the Alps, the renewed growth of Calderone Glacier just after 2565–2155 cal. BC
636 (med. prob.: 2370 cal. BC), as shown by a soil reworked by the glacier tongue and
637 incorporated into a moraine, is considered as marking the onset of the Neoglacial in the
638 Apennines (**Giraudi, 2005**).
639 Finally, between the '4.2 ka advance' and the culmination of the next period of glacier
640 advance (Löbben Advance Period, see Section 6.3.1), a marked and possibly multi-phased
641 retreat occurred. Morteratsch Glacier reached a position at least as retracted as c. AD 2000
642 before to advance over this extent after 2195–1775 cal. BC (med prob.: 1995 cal. BC;
643 **Holzhauser, 2010**). Renewed peat growth at Pasterze Glacier between 1935–1745 cal. BC
644 (med. prob.: 1835 cal. BC) and 1625–1445 cal. BC (med prob.: 1540 cal. BC) indicates multi-
645 secular ice free conditions (extent < AD 2007) at the beginning of the Löbben Advance
646 Period in the forefield of this slow reacting glacier (**Kellerer-Pirklbauer and Drescher-**
647 **Schneider, 2009**). Mostly-glacier-hostile conditions characterizing this period are also clearly
648 reflected by the temperature-sensitive $\delta^{18}O$ record from high-elevation speleothems (**Fig. 6a**)
649 as well as by the Mer de Glace and Schnidejoch records (**Fig. 7a/b**)
650
651 *6.2. The '4.2 ka advance' in the Northern Hemisphere*
652
653 Glacier advances coeval with our data and marking the onset of the local Neoglacial were
654 also reported from Greenland (**Balascio et al., 2015**), Svalbard (**van der Bilt et al., 2015**)
655 Iceland (**Striberger et al., 2012**; **Larsen et al., 2012**) and Scandinavia (**Bakke et al., 2010**;
656 **Vasskog et al., 2012**; **Jansen et al., 2016**), based on lake-sediments. Outside of the North
657 Atlantic realm, numerous glacially-sheared *in situ* stumps and some wood mats were
658 radiocarbon-dated around 4.2 ka in the Canadian coastal cordilleras (see review in **Menounos**
659 **et al., 2008;** see also **Menounos et al., 2009**; **Harvey et al., 2012**; **Maurer et al., 2012**;
660 **Osborn et al., 2013**; **Mood and Smith, 2015**; **Luckman et al., 2017**). In this area, the
661 advance probably did not reach Holocene maxima but was quite prominent, at least similar to
662 the AD 1940 extent (e.g. **Maurer et al., 2012**). Glacier chronologies from Alaska show a

prominent advance dated between 4.6 and 4.0 ka marking the onset of the local Neoglacial (**Krivicich, 2009**; **McKay and Kaufman, 2009**; **Badding et al., 2013**), with an ELA depression around 4.2 ka comparable to the one of the Holocene maxima (**Boldt et al., 2012**) and a frontal position exceeding the LIA moraines (**Badding et al., 2013**). A significant increase in snow cover, persisting almost continuously from that time up to the 20th century warming, has also been evidenced from wood remnants buried by perennial snow patches in the Colorado Front Range (**Benedict et al., 2008**). At high latitudes, current ice-cap melt rates were found to be without analog since 4.2 ka in the Canadian Arctic (**Fisher et al., 2012**; **Miller et al., 2013**; **Margreth et al., 2014**). This whole set of data point to a hemispheric climatic event leading to prominent glacier advances in most Northern Hemisphere mountain ranges.

Fig 7.

6.3. Other EPM Neoglacial advances in the Alpine context

6.3.1. The '3.6 ka advance'

At Bonnepierre Glacier and likely also at Rateau Glacier, evidence is provided for a prominent and multi-phased glacier advance which culminated at 3.66 ± 0.09 ka (1660 ± 90 BC; mean age of the three moraines at the two sites). This advance is coeval with the so-called 'Löbben' period in the Alps (Löbben Advance Period, LAP; c. 1900–1450 BC; **Patzelt and Bortenschlager, 1973**; **Nicolussi et al., 2006**). This result is in line with the extensive body of work that reports dating of LAP moraines in the Alps (**Fig. 6d-f**; see review in **Holzhauser 2010** and **Moran et al., 2017**; see also **Le Roy et al., 2015**). At several sites, these moraines are the first lateral ones preserved inboard of the Lateglacial/early Holocene positions (e.g. **Wipf, 2001**; **Schimmelpfennig et al., 2012**) and more rarely the most down-valley preserved Neoglacial frontal ridges (**Wipf, 2001**; **Moran et al., 2017**). Our tentative interpretation of the Rateau Glacier dating results implies that the three outermost ridges MA to MC (on which the resulting boulder ages are most likely underestimated; **Fig. 3a** and **4a**) either pre-date the LAP or were deposited during the LAP shortly before moraine MD. In the Swiss Alps, the Tschingel Glacier forefield gives evidence for a multi-phased LAP, with four ridges attributed to this period (**Wipf, 2001**). The higher climate sensitivity of Rateau Glacier

with respect to Bonnepierre Glacier (see Section 3) could explain why four ridges would have been deposited during the LAP by the first, and only two by the latter.

Our TCN ages agree remarkably with dendro-dating evidence for the time span of the LAP culmination in the Alps, placed between 1660 and 1545 BC from analyses carried out on tens of glacially-buried subfossil logs (**Fig. 7a**; **Nicolussi and Patzelt, 2001**; **Le Roy et al., 2015**). Similarly, the glacio-lacustrine record from Lake Bramant, located 20 km north of the EPM, shows a rise in clastic sedimentation between c. 1700 and 1400 BC indicating a contemporaneous advance of Saint Sorlin Glacier (**Fig. 7e**; **Guyard et al., 2013**). Further evidence comes from the radiocarbon ages of archeological finds on Schnidejoch Pass, which drop drastically at 3.6 ka, likely reflecting a glacier-induced cessation of the pass traverse (**Fig. 7b**; **Hafner and Schwörer, 2017**). At Tsidjiore Nouve Glacier in the western Swiss Alps, recalculation of the age of ARO-12 – the tallest and most ice-distal boulder from the LAP-aged moraine dated by **Schimmelpfennig et al. (2012)** – with the PR used in this study yields an age of 3.60 ± 0.11 ka (1600 ± 110 BC). Alike, recalculation of the data from frontal moraine M2A at Längental Glacier, western Austria (**Moran et al., 2017**), yields a mean age of 3.54 ± 0.18 ka (1540 ± 180 BC). This means that deposition of these ridges was synchronous with that of our dated ridges in the EPM and consistent with independent (dendro-based) evidence constraining the culmination of the LAP.

Finally, Alpine paleoclimatic proxies show unambiguously a sharp drop in temperature between 3.6 and 3.5 ka (**Fig. 6a**; **Fohlmeister et al., 2013;** see also **Le Roy et al., 2015**, their Fig. 8f), also reflected in the treeline record (**Fig. 6b**; **Nicolussi et al., 2005**).

On a global scale, firm evidence now indicate that glacier advances contemporary to the Löbben Advance Period occurred at other Northern Hemipshere locations (**Osborn et al., 2013**; **Luckman et al., 2017**; **Schweinsberg et al., 2017**)

6.3.2. The '2.1 ka advance'

At Bonnepierre Glacier, the next prominent advance for which evidence is preserved took place in the late Iron Age/early Roman times, at 2.09 ± 0.1 ka (90 ± 100 BC). Little geomorphic evidence yet exist in the Alps for an advance occurring at that time. To our knowledge, only two sites provided evidence for a large advance in the first century BC. In the Austrian Alps, Gepatsch Glacier advanced beyond its AD 1930 extent around 200 cal. BC–130 cal. AD (median prob.: 35 cal. BC; **Patzelt, 1995**; **Nicolussi and Patzelt, 2001**). In the French Alps, Argentière Glacier likely achieved advanced positions after 174+ BC as shown by a log embedded in till 15 m below the moraine crest (dendro-date for the tree

729 ARG04; **Le Roy, 2012**). At the nearby glacier Mer de Glace, indirect evidence based on two
730 detrital logs could indicate that an advance occurred after 87+ BC (**Fig. 7a**). Moreover, this
731 period stands out in the glacio-lacustrine record of Lake Bramant, reflecting enhanced glacial
732 activity centred on 70 cal. BC (**Fig. 7e**; **Guyard et al., 2013**). Minimum-limiting temporal
733 constraints for the '2.1 ka advance' include the first germination dates of subfossil trees
734 retrieved from the Mer de Glace lateral moraine, recorded from 23 BC (**Fig. 7a**). These dates
735 probably reflect the shift to warmer conditions at the onset of the Roman Era. Likewise,
736 radiocarbon age PDFs of the archeological artefacts found at Schnidejoch Pass start around
737 2.15 ka, supporting a change from glacier-friendly to glacier-hostile conditions at that time
738 (**Fig. 7b**).
739 Possible drivers for the '2.1 ka advance' could be the strong rise in spring (April, May,
740 June) precipitation that occurred around 100 BC **(Büntgen et al., 2011)** associated with
741 slightly below average summer (June, July, August) temperatures (**Luterbacher et al., 2016**).
742 Shortly after, a marked drop of summer temperature occurred at 44 BC (**Büntgen et al.,**
743 **2011**). This cooling episode was caused by the third largest volcanic event of the last 2,500
744 yrs, leading to one of the coldest decade of the Late Holocene (**Sigl et al., 2015**).
745
746 *6.3.3. The '1.3 ka advance'*
747 Another Neoglacial maximum might be represented by the single boulder dated to 1.31 ±
748 0.17 ka (AD 690 ± 170) at Lautaret Glacier. This dating coincides with the regionally called
749 'Göschenen II' advance period (GII; c. 200-850 AD; **Zoller et al., 1966**). GII glacier
750 advances surpassed the LIA extent at a number of locations in the Alps, e.g. at Rhône Glacier
751 (**Zumbühl and Holzhauser, 1988**) and Simony Glacier (**Patzelt and Bortenschlager, 1973**;
752 **Patzelt, 1974**). At Lautaret Glacier, the deposition pattern is constrained by topography as the
753 composite moraine is backed against the rock wall (**Fig. 3b** and **4b**). It is therefore possible
754 that immediately preceding Neoglacial advances were of nearly the same magnitude. Within
755 uncertainties, the Lautaret Glacier Neoglacial maximum is contemporary with the prominent
756 GII advance of Mer de Glace, dendro-dated to AD 606+, with an extent that had reached
757 approximately the AD 1870 level (**Le Roy et al., 2015**). First millennium prominent detrital
758 peaks in the glacio-lacustrine records presented on **Fig. 7d/e** could also be linked to this
759 advance, given that both age models are loosely constrained on this time period.
760 The end of the GII, also called the Late Antique Little Ice Age (**Büntgen et al., 2016**),
761 was characterized by a volcanic-induced cooling that started in AD 536 (**Toohey et al., 2016**).
762 Cold conditions with at least hemispheric relevance persisted then until AD 660 (**Büntgen et**

al., 2016), possibly responsible for the low juvenile growth of the Eta01 tree near the Etages Glacier forefield (Fig. 5).

6.3.4. The '0.9 ka advance'

Moraine M1 at Etages Glacier is the only site where a pre-LIA frontal moraine has been dated in the EPM. The age of 0.92 ± 0.02 ka (AD 1085 ± 20), which is constrained by two consistent TCN ages and by independent evidence as well (see Section 5.2.4), agrees with a deposition during a High Medieval Advance (HMA, c. 1100–1250 AD; **Nicolussi et al., 2006**).

In the EPM, evidence for a HMA is also present in the sediment record of proglacial Lake Muzelle (**Fouinat et al., 2017**; see **Fig. 1a** for location). In this lake, clastic sedimentation increased towards the end of the MCA and peaked a first time at c. AD 1070-1080, in remarkable agreement with our TCN age (**Fig. 7d**). After a drop centred on 1150, a larger clastic excursion occurred between c. AD 1240 and 1305, marking the onset of the LIA (**Fig. 7d**). Overall, this pattern is very similar to other lacustrine detrital record from the French Alps partly controlled by glacier size (**Fig. 7e**; **Arnaud et al., 2012**; **Guyard et al., 2013**).

Geomorphic evidence for a HMA has been identified at numerous sites in the Alps. Although it does not represent a Neoglacial maximum, significant advances have been proven for several large (> 10 km^2) glaciers (see **Holzhauser, 2010** and **Le Roy et al., 2015**). When accurate dendro-dates are available, they indicate advances that peaked during the early to late 12^{th} century (between AD 1125 and 1186), depending on glacier response times. At Mer de Glace, this advance is well-constrained between AD 1120 and 1178, an interval during which the glacier grew from the AD 1890 level to the AD 1870 level (**Le Roy et al., 2015**). By AD 1100, the slow-reacting Aletsch Glacier was advancing over its AD 1926 extent (**Holzhauser et al., 2005**). Because of its smaller size, Etages Glacier could have reached a maximum slightly earlier than large glaciers, in response to a temperature drop spanning the second half of the 11^{th} century (**Büntgen et al., 2006**; **Millet et al., 2009**) and this position could have been more advanced relative to large glaciers.

Conclusions

We presented the first numerical constraints on Neoglacial glacier advances in the French Alps outside of the Mont Blanc Massif. Our results indicate that large advances, almost

similar to the LIA maximum, occurred repeatedly – at least five times – since c. 4.2 ka in the Ecrins-Pelvoux massif.

Some advances dated here match the timing of widely dated Neoglacial advances in the Alps, like the Löbben Advance Period, whose culmination has occurred at c. 3.6-3.5 ka, and the Göschenen II advance, that peaked around 1.4 ka. The multi-phased nature of the LAP, first identified in the central and eastern Alps, is confirmed here, as several moraines were attributed to this period in the EPM.

Novel key findings are:

- The first direct dating of a moraine contemporary with the '4.2 ka event' in the Alps, an event recognized as a key marker for the subdivision of the Holocene (**Walker et al., 2012**).
- The identification of an extensive advance occurring at the beginning of the Roman Era, around 2.1 ka. To our knowledge, no other moraine ridges contemporary with this advance were previously dated in the Alps, although evidence for concomitant glacial activity is present in lateral moraine stratigraphy at least at two other sites, as well as in some glacio-lacustrine records.
- The characterization of a High Medieval Advance that represents a Neoglacial maximum during the Medieval Climate Anomaly is noteworthy as the magnitude of this advance is smaller at the other sites where it was dated in the Alps.

Taking into account previous work carried out in the western Alps (**Le Roy et al., 2015**) c. 12 periods of glacier advance have now been identified during the Neoglacial with no more than 5 centuries between two consecutive events.

The combination of multiple sites allowed us to identify more Neoglacial glacier advances that this would have been possible at a single site. However, firm conclusions regarding the unequivocal climatic origin of most of the glacier advances could not be drawn from our data given that only one period of advance has been dated at two sites (LAP at Bonnepierre and Rateau Glaciers). Nevertheless our dated advances are all consistent with an array of paleoclimatic evidence (see Sections 6.1.1 and 6.3), which support their probable climatic origin.

Finally, in the EPM (and most generally in the Alps), geomorphological evidence for Neoglacial advances that pre-date the LIA are mostly preserved in lateral position in sectors that were not overtopped during the LIA. This is due to the progressive channelization of ice

flow by lateral moraines in the course of the Neoglacial. Attention must be drawn on the preservation of these landforms. In non-stabilized sectors, as erosion proceeds, some of the ridges dated in this study will disappear in a near future due to moraine backwall retreat (e.g. the innermost ridges at Bonnepierre Glacier). This will lead to a net loss of a valuable paleoclimatic archive.

Acknowledgements

Most of this study was carried out during the PhD project of MLR funded by the French Ministry of Higher Education and Research (MESR grant 2008-11). Analytical support was provided by the Institut National des Sciences de l'Univers (INSU) LEFE/EVE program (AO2011-651683). The authors acknowledge the Ecrins National Park for sampling authorization (n° 307/2010). We are grateful to Arnaud Pêcher (ISTerre) for identification of the rock samples, and to Riccardo Vassallo (ISTerre) and Georges Aumaître (CEREGE) for their help during preparation of the ^{10}Be target. Kurt Nicolussi (Institute of Geography, University of Innsbruck) helped in crossdating the eta01 tree-ring series and kindly provided glacier data for Figure 6. ^{10}Be measurements were performed at the ASTER AMS national facility (CEREGE, Aix en Provence), which is supported by the INSU/CNRS, the ANR through the 'Projets thématiques d'excellence' program for the 'Equipements d'excellence' ASTER-CEREGE action, IRD and CEA. We thank the two anonymous reviewers whose relevant remarks have improved this manuscript.

References

Allix A., Benevent E., Blanchard R., Flusin G., Gignoux M., Jacob C., 1927. Observations glaciologiques faites en Dauphiné jusqu'en 1924, récapitulées et partiellement éditées. Études Glaciologiques, tome 6, Ministère de l'Agriculture, 1–141.

Andresen C.S., Björck S., Rundgren M., Conley D.J., Jessen C., 2006. Rapid Holocene climate changes in the North Atlantic: evidence from lake sediments from the Faroe Islands. Boreas 35, 23–34.

Arnaud F., Révillon S., Debret M., Revel M., Chapron E., Jacob J., Giguet-Covex C., Poulenard J., Magny M., 2012. Lake Bourget regional erosion patterns reconstruction reveals Holocene NW European Alps soil evolution and paleohydrology. Quaternary Science Reviews 51, 81–92.

Arnold M., Merchel S., Bourlès D., Braucher R., Benedetti L., Finkel R.C., Aumaître G., Gottdang A., Klein M., 2010. The French accelerator mass spectrometry facility ASTER: Improved

performance and developments. Nuclear Instruments and Methods in Physics Research B 268, 1954–1959.

Auer I., Böhm R., Jurkovi A., Lipa W., Orlik A., Potzmann R., Schöner W., Ungersböck M., Matulla C., Briffa K., Jones P., Efthymiadis D., Brunetti M., Nanni T., Maugeri M., Mercalli L., Mestre O., Moisselin J.-M., Begert M., Müller-Westermeier G., Kveton V., Bochnicek O., Stastny P., Lapin M., Szalai S., Szentimrey T., Cegnar T., Dolinar M., Gajic-Capka M., Zaninovic K., Majstorovic Z., Nieplova E., 2007. HISTALP - historical instrumental climatological surface time series of the Greater Alpine Region. Int. J. Climatol. 27, 17–46.

Badding M.E., Briner J.P., Kaufman D.S., 2013. ^{10}Be ages of late Pleistocene deglaciation and Neoglaciation in the north-central Brooks Range, Arctic Alaska. Journal of Quaternary Science 28, 1, 95–102.

Bajard M., Sabatier P., David F., Develle A-L., Reyss J-L., Fanget B., Malet E., Arnaud D., Augustin L., Crouzet C., Poulenard J., Arnaud F., 2016. Erosion record in Lake La Thuile sediments (Prealps, France): Evidence of montane landscape dynamics throughout the Holocene. The Holocene 26, 3, 350–364.

Bakke J., Dahl S.O., Paasche Ø., Simonsen J.R., Kvisvik B., Bakke K., Nesje A., 2010. A complete record of Holocene glacier variability at Austre Okstindbreen, northern Norway: an integrated approach. Quaternary Science Reviews 29, 1246–1262.

Balascio N.L., D'Andrea W.J., Bradley R.S., 2015. Glacier response to North Atlantic climate variability during the Holocene. Climate of the Past 11, 1587–1598.

Balco G., Stone J.O., Lifton N.A., Dunai, T.J., 2008. A complete and easily accessible means of calculating surface exposure ages or erosion rates from ^{10}Be and ^{26}Al measurements. Quaternary Geochronology 3, 174–195.

Balco G., Briner J., Finkel R.C., Rayburn J., Ridge J.C., Schaefer J.M., 2009. Regional beryllium-10 production rate calibration for late-glacial northeastern North America. Quaternary Geochronology 4, 93–107.

Ballantyne C.K., Stone J.O., 2012. Did large ice caps persist on low ground in north-west Scotland during the Lateglacial Interstade? Journal of Quaternary Science 27, 3, 297–306.

Barber K.E., Chambers F.M., Maddy D., 2003. Holocene palaeoclimates from peat stratigraphy: macrofossil proxy climate records from three oceanic raised bogs in England and Ireland Quaternary Science Reviews 22, 521–539.

Barbier R., Barféty J.C., Bordet P., 1976. Notice de la carte géologique de la France à 1/50 000^{e}, feuille 798 (La Grave). Bureau de Recherches Géologiques et Minière, Orléans.

Barféty J-C, Pêcher A., 1984. Notice de la carte géologique de la France à 1/50 000^{e}, feuille 822 (Saint Christophe en Oisans). Bureau de Recherches Géologiques et Minière, Orléans.

Baroni C., Orombelli G., 1996. The Alpine 'Iceman' and Holocene climatic change. Quaternary Research 46, 78–83.

902 Barr I.D., Lovell H., 2014. A review of topographic controls on moraine distribution. Geomorphology
903 226, 44–64.
904 Benedict J.B., Benedict R.J., Lee C.M. Staley D.M., 2008. Spruce trees from a melting ice patch:
905 evidence for Holocene climatic change in the Colorado Rocky Mountains, USA. The Holocene
906 18, 7, 1067–1076.
907 Boldt B.R., Kaufman D.S., Briner J.P., 2012. A lacustrine record of middle- to late-Holocene
908 glaciation from Kurupa Lake, north-central Brooks Range, Arctic Alaska. 42nd Arctic Workshop,
909 Colorado, USA, Program and Abstracts 2012, 17–21.
910 Boldt B.R., Kaufman D.S., McKay N.P., Briner J.P., 2015. Holocene summer temperature
911 reconstruction from sedimentary chlorophyll content, with treatment of age uncertainties, Kurupa
912 Lake, Arctic Alaska. The Holocene 25, 4, 641–650.
913 Bonaparte R., 1891. Les variations périodiques des glaciers français. Annuaire du C.A.F., 17e et 18e
914 vol., 1890–1891.
915 Bonaparte R., 1892. Mesure des variations de longueur des glaciers du Dauphiné (massif du Pelvoux).
916 Paris, Impr. Gauthier, 3 pp.
917 Bonet R., Arnaud F., Bodin X., Bouche M., Boulangeat I., Bourdeau P., Bouvier M., Cavalli L.,
918 Choler P., Delestrade A., Dentant C., Dumas D., Fouinat L., Gardent M., Lavergne S.,
919 Naffrechoux E., Nellier Y., Perga M-E., Sagot C., Senn O., Thuiller W., 2016. Indicators of
920 climate: Ecrins National Park participates in long-term monitoring to help determine the effects of
921 climate change. Eco.mont 8, 1, 44–52.
922 Bourgeat S., 1990. Eboulements et écroulements dans le bassin versant du Vénéon (massif des Ecrins,
923 Isère). Revue de Géographie Alpine 28, 1/2/3, 11–23.
924 Borchers B., Marrero S., Balco G., Caffee M., Goehring B., Lifton N., Nishiizumi K., Phillips F.,
925 Schaefer J., Stone J., 2016. Geological calibration of spallation production rates in the CRONUS-
926 Earth project. Quaternary Geochronology 31, 188–198.
927 Briner J.P., Young N.E., Goehring B.M., Schaefer J.M., 2012. Constraining Holocene ^{10}Be production
928 rates in Greenland. Journal of Quaternary Science 27, 2–6.
929 Brisset E., Miramont C., Guiter F., Anthony E., Tachikawa K., Poulenard J., Arnaud F., Delhon C.,
930 Meunier J-D., Edouard Bard E., Suméra F., 2013. Non-reversible geosystem destabilisation at
931 4200 cal. BP: Sedimentological, geochemical and botanical markers of soil erosion recorded in a
932 Mediterranean alpine lake. The Holocene 23, 12, 1863–1874.
933 Bronk Ramsey C. and Lee S., 2013. Recent and planned developments of the Program OxCal.
934 Radiocarbon 55, 720–730.
935 Brown E.T., Edmond J.M., Raisbeck G.M., Yiou F., Kurz M.D., Brook E.J., 1991. Examination of
936 surface exposure ages of Antarctic moraines using *in-situ* produced ^{10}Be and ^{26}Al. Geochimica et
937 Cosmochimica Acta 55, 2269–2283.

938 Büntgen U., Frank D.C., Nievergelt D., Esper J., 2006. Summer temperature variations in the
939 European Alps, A.D. 755–2004. Journal of Climate 19, 5606–5623.
940 Büntgen U., Tegel W., Nicolussi K., McCormick M., Frank D., Trouet V., Kaplan J., Herzig F.,
941 Heussner U., Wanner H., Luterbacher J., Esper J., 2011. 2500 years of European climate
942 variability and human susceptibility. Science 331, 578–582.
943 Büntgen U., Myglan V.S., Ljungqvist F.C., McCormick M., Di Cosmo N., Sigl M., Jungclaus J.,
944 Wagner S., Krusic P.J., Esper J., Kaplan J.O., de Vaan M.A.C., Luterbacher J., Wacker L., Tegel
945 W., Kirdyanov A.V., 2016. Cooling and societal change during the Late Antique Little Ice Age
946 from 536 to around 660 AD. Nature Geoscience 9, 231–236.
947 Chenet M., Brunstein D., Jomelli V., Roussel E., Rinterknecht V., Mokadem F., Biette M., Robert V.,
948 Leanni L., ASTER Team, 2016. ^{10}Be cosmic-ray exposure dating of moraines and rock avalanches
949 in the Upper Romanche valley (French Alps): Evidence of two glacial advances during the Late
950 Glacial/Holocene transition. Quaternary Science Reviews 148, 209–221.
951 Chmeleff J., von Blanckenburg F., Kossert K., Jakob J., 2010. Determination of the ^{10}Be half-life by
952 multicollector ICP-MS and liquid scintillation counting. Nuclear Instruments and Methods in
953 Physics Research B 268 (2), 192–199.
954 Claude A., Ivy-Ochs S., Kober F., Antognini M., Salcher B., Kubik P.W., 2014. The Chironico
955 landslide (Valle Leventina, southern Swiss Alps): age and evolution. Swiss Journal of
956 Geosciences 107, 273–291
957 Colas A., 2000. Recherches géomorphologiques en Vallouise. PhD Thesis. Université de Lille 1, 291
958 pp.
959 Cossart E., 2011. Mapping Glacier Variations at Regional Scale through Equilibrium Line Altitude
960 Interpolation: GIS and Statistical Application in Massif des Écrins (French Alps). Journal of
961 Geographic Information System 3, 232–241.
962 Cossart E., Fort M., Jomelli V., Grancher D., 2006. Les variations glaciaires en Haute Durance
963 (Briançonnais, Hautes Alpes) depuis la fin du XIX^{e} siècle : mise au point d'après les documents
964 d'archive et la lichénométrie. Quaternaire 17, 1, 75–92.
965 Cossart E., Bourlès D., Braucher R., Carcaillet J., Fort M., Siame L., 2011. L'englacement du haut
966 bassin durancien (Alpes françaises du sud) du Dernier Maximum Glaciaire à l'Holocène : synthèse
967 chronologique. Géomorphologie: Relief, Processus, Environnement 2, 5–32.
968 Coûteaux M., 1983a. Fluctuations glaciaires de la fin du Würm dans les Alpes françaises, établies par
969 des analyses polliniques. Boreas 12, 1, 35–56.
970 Coûteaux M., 1983b. La déglaciation du vallon de la Lavey (Vallée du Vénéon, massif des Ecrins,
971 Isère), S.H.F., Section de Glaciologie, compte-rendu de la séance de Grenoble (Mars 1983), 1–13.
972 Coûteaux M., 1984. Présence, datages et signification phytosociologique de macrorestes de *Pinus* et
973 de pollens de *Pinus cembra* L. à 2050 m dans le vallon de la Lavey (massif des Écrins, Isère,
974 France). Revue de Paleobiologie. NS, 55–62.

Deline P., Orombelli G., 2005. Glacier fluctuations in the western Alps during the Neoglacial as indicated by the Miage morainic amphiteatre (Mont Blanc massif, Italy). Boreas 34, 456–467.

Delunel R., 2010. Evolution géomorphologique du massif des Ecrins-Pelvoux depuis le Dernier Maximum Glaciaire – Apports des nucléides cosmogéniques produits *in-situ*. PhD Thesis, Université Joseph Fourier, Grenoble, 261 pp.

Delunel R., Hantz D., Braucher R., Bourlès D.L., Schoeneich P., Deparis J., 2010a. Surface exposure dating and geophysical prospecting of the Holocene Lauvitel rock slide (French Alps). Landslides 7, 393–400.

Delunel R., van der Beek P., Carcaillet J., Bourlès D., 2010b. Deglaciation chronology of the Ecrins-Pelvoux massif (French Western Alps) revealed from new ^{10}Be and ^{26}Al Cosmic Ray Exposure ages. Geophysical Research Abstracts 12, EGU2010-9320.

Delunel R., van der Beek P., Bourlès D., Carcaillet J., Schlunegger F., 2014a. Transient sediment supply in a high-altitude Alpine environment evidenced through a ^{10}Be budget of the Etages catchment (French Western Alps). Earth Surface Processes and Landforms 39, 7, 890–899.

Delunel R., Bourlès D.L., van der Beek P.A., Schlunegger F., Leya I., Masarik J., Paquet E., 2014b. Snow shielding factors for cosmogenic nuclide dating inferred from long-term neutron detector monitoring. Quaternary Geochronology 24, 16–26.

Di Costanzo H., Hofmann F-M., 2016. Le retrait du glacier du Drac Blanc (massif des Écrins, Alpes françaises). Méditerranée. URL : http:// mediterranee.revues.org/7796.

Drescher-Schneider R., Kellerer-Pirklbauer A., 2008. Gletscherschwund einst und heute. Neue Erkenntnisse zur holozänen Vegetations- und Klimageschichte der Pasterze (Hohe Tauern, Österreich). In: J.M. Reitner, M.C. Fiebig, C. Neugebauer-Maresch, M. Pacher und V. Winiwarter (Eds.): Veränderter Lebensraum - Gestern, heute und morgen. Tagung DEUQUA, 31. August - 6. September 2008, Wien. Abhandlungen Geologischen Bundesanstalt 62, 45–51.

Dumont T., Champagnac J.D., Crouzet C., Rochat P., 2008. Multistage shortening in the Dauphiné zone (French Alps): the record of Alpine collision and implications for pre-Alpine restoration. Swiss Journal of Geosciences 101, 89–110.

Eckstein J., Leuschner H.H., Giesecke T., Shumilovskikh L., Bauerochse A., 2010. Dendroecological investigations at Venner Moor (northwest Germany) document climate-driven woodland dynamics and mire development in the period 2450-2050 BC. The Holocene 20, 2, 231–244.

Edouard J-L., 1978. La glaciation dans le massif de l'Oisans. Contribution à la connaissance des fluctuations glaciaires postwürmiennes. PhD Thesis, Université de Grenoble, 329 pp.

Fenton C.R., Hermanns R.L., Blikra L.H., Kubik P.W., Bryant C., Niedermann S., Meixner A., Goethals M.M., 2011. Regional ^{10}Be production rate calibration for the past 12 ka deduced from the radiocarbondated Grøtlandsura and Russenes rock avalanches at 69° N, Norway. Quaternary Geochronology 6, 437–452.

1011 Fisher D., Zheng J., Burgess D., Zdanowicz C., Kinnard C., Sharp M., Bourgeois J., 2012. Recent melt
1012 rates of Canadian arctic ice caps are the highest in four millennia. Global and Planetary Change
1013 84-85, 3–7.
1014 Fohlmeister J., Vollweiler N., Spötl C., Mangini A., 2013. COMNISPA II: Update of a mid-European
1015 isotope climate record, 11 ka to present. The Holocene 23, 5, 749–754.
1016 Fouinat L., Sabatier P., Arnaud F., Chaumillon E., Schoeneich P., 2013. Age et modalités de
1017 l'effondrement à l'origine du lac de Lauvitel, (vallée de l'Oisans, 1530 m). Apports d'une approche
1018 couplée : datations cosmogéniques, sismique réflexion et carottages lacustres. 14e congrès français
1019 de sédimentologie, Nov. 2013, Paris.
1020 Fouinat L., Sabatier P., Poulenard J., Etienne D., Crouzet C., Develle A-L., Doyen E., Malet E., Reyss
1021 J-L., Sagot C., Bonet R., Arnaud F., 2017. One thousand seven hundred years of interaction
1022 between glacial activity and flood frequency in proglacial Lake Muzelle (western French Alps).
1023 Quaternary Research 87, 407–422.
1024 Francou B., 1981. Géodynamique des éboulis et formes associées de la Combe de Laurichard. PhD
1025 Thesis, Université de Grenoble, 153 pp.
1026 Furrer G., Burga C., Gamper M., Holzhauser H., Maisch M., 1987. Zur Gletscher-, Vegetations- und
1027 Klimageschichte der Schweiz seit der Späteiszeit. Geographica Helvetica 42, 61–91.
1028 Gabrielli P., Barbante C., Bertagna G., Bertó M., Binder D., Carton A., Carturan L., Cazorzi F., Cozzi
1029 G., Dalla Fontana G., Davis M., De Blasi F., Dinale R., Dragà G., Dreossi G., Festi D., Frezzotti
1030 M., Gabrieli J., Galos S. P., Ginot P., Heidenwolf P., Jenk T. M., Kehrwald N., Kenny D., Magand
1031 O., Mair V., Mikhalenko V., Lin P. N., Oeggl K., Piffer G., Rinaldi M., Schotterer U.,
1032 Schwikowski M., Seppi R., Spolaor A., Stenni B., Tonidandel D., Uglietti C., Zagorodnov V.,
1033 Zanoner T., Zennaro P., 2016. Age of the Mt. Ortles ice cores, the Tyrolean Iceman and glaciation
1034 of the highest summit of South Tyrol since the Northern Hemisphere Climatic Optimum. The
1035 Cryosphere 10, 2779–2797.
1036 Gardent M., Rabatel A., Dedieu J.P., Deline P., 2014. Multitemporal glacier inventory of the French
1037 Alps from the late 1960s to the late 2000s. Global and Planetary Change 120, 24–37.
1038 Gibbons A.B., Megeath J.D., Pierce K.L., 1984. Probability of moraine survival in a succession of
1039 glacial advances. Geology 12, 327–330.
1040 Giraudi C., 2005. Middle to Late Holocene glacial variations, periglacial processes and alluvial
1041 sedimentation on the higher Apennine massifs (Italy). Quaternary Research 64, 176–184.
1042 Goehring B.M, Lohne Ø.S., Mangerud J., Svendsen J.I., Gyllencreutz R., Schaefer J., Finkel R., 2012.
1043 Late Glacial and Holocene ^{10}Be production rates for western Norway. Journal of Quaternary
1044 Science 27, 89–96.
1045 Gosse J.C., 2005. The contributions of cosmogenic nuclides to unravelling alpine paleo-glacier
1046 histories. In: Huber U.M., Bugmann H.K.M., Reasoner M.A. (Eds.), Global Change and Mountain
1047 Regions: an Overview of Current Knowledge. Springer, Dordrecht, 39–50.

1048 Gross G., Kerschner H., and Patzelt G., 1977. Methodische Untersuchungen uber die Schneegrenze in
1049 alpinen Gletschergebieten. Zeitschrift für Gletscherkunde und Glazialgeologie 7, 223–251.
1050 Guyard H., Chapron E., St-Onge G., Labrie J., 2013. Late-Holocene NAO and oceanic forcing on
1051 high-altitude alpine proglacial sedimentation (Lake Bramant, Western French Alps). The
1052 Holocene 23, 1163–1172.
1053 Hafner A., Schwörer C., 2017. Vertical mobility around the high-alpine Schnidejoch Pass. Indications
1054 of Neolithic and Bronze Age pastoralism in the Swiss Alps from paleoecological and
1055 archaeological sources. Quaternary International, https://doi.org/10.1016/j.quaint.2016.12.049
1056 Harvey J.E., Smith D.J., Laxton S., Desloges J. Allen S., 2012. Mid-Holocene glacier expansion
1057 between 7500 and 4000 cal. yr BP in the British Columbia Coast Mountains, Canada. The
1058 Holocene 22, 9, 975–985.
1059 Heyman J., Applegate P.J., Blomdin R., Gribenski N., Harbor J.M., Stroeven A.P., 2016. Boulder
1060 height – exposure age relationships from a global glacial ^{10}Be compilation. Quaternary
1061 Geochronology 34, 1–11.
1062 Hoelzle M., Chinn T.J., Stumm D., Paul F., Zemp M., Haeberli W., 2007. The application of inventory
1063 data for estimating characteristics of and regional past climate-change effects on mountain
1064 glaciers: a comparision between the European Alps and the New Zealand Alps. Global and
1065 Planetary Change 56, 69–82.
1066 Hoffmann T., Lang A., Dikau R., 2008. Holocene river activity: analysing ^{14}C-dated fluvial and
1067 colluvial sediments from Germany, Quaternary Science Reviews 27, 2031–2040.
1068 Holzhauser H., 2007. Holocene glacier fluctuations in the Swiss Alps. In Mordant C, Richard H,
1069 Magny M. (Eds). Environnements et cultures à l'Âge du Bronze en Europe occidentale, Comité
1070 des travaux historiques et scientifiques (CTHS), Paris, 29–43.
1071 Holzhauser H., 2010. Zur geschichte des Gornergletschers – Ein puzzle aus historischen dokumenten
1072 und fossilen hölzern aus dem gletschervorfeld. Geographica Bernensia, G 84. Institute of
1073 Geography, University of Bern, 253 pp.
1074 Holzhauser H., Magny M., Zumbühl H.J., 2005. Glacier and lake-level variations in west-central
1075 Europe over the last 3500 years. The Holocene 15, 6, 789–801.
1076 Jacob C., Flusin G., 1905. Etude sur le glacier Noir et le glacier Blanc dans le massif du Pelvoux :
1077 [rapport sur les observations rassemblées en août 1904 dans les Alpes du Dauphiné].
1078 Jansen H.L., Simonsen J.R., Dahl S.O., Bakke J., Nielsen P.R., 2016. Holocene glacier and climate
1079 fluctuations of the maritime ice cap Høgtuvbreen, northern Norway. The Holocene 26, 5, 736–
1080 755.
1081 Joerin U., Stocker T.F., Schlüchter C., 2006. Multicentury glacier fluctuations in the Swiss Alps. The
1082 Holocene 16, 5, 697–704.

1083 Joerin U., Nicolussi K., Fischer A., Stocker T.F., Schlüchter C., 2008. Holocene optimum events
1084 inferred from subglacial sediments at Tschierva Glacier, Eastern Swiss Alps. Quaternary Science
1085 Reviews 27, 337–350.
1086 Jóhannesson T., Raymond C., Waddington E., 1989. Time-scale for adjustment of glaciers to changes
1087 in mass balance. Journal of Glaciology 35, 121, 355–369.
1088 Kellerer-Pirklbauer A., Drescher-Schneider R., 2009. Glacier fluctuation and vegetation history during
1089 the Holocene at the largest glacier of the Eastern Alps (Pasterze Glacier, Austria): New insight
1090 based on recent peat findings. Proceedings of the 4th Symposium of the Hohe Tauern National
1091 Park for Research in Protected Areas, Kaprun, Austria, September 2009, 151–155.
1092 Kilian W., 1900. Observations sur les variations des glaciers et l'enneigement dans les Alpes
1093 dauphinoises de 1890 à 1899. Allier, Grenoble, 231 pp.
1094 Kirkbride M.P., Winkler S., 2012. Correlation of Late Quaternary moraines: Impact of climate
1095 variability, glacier response, and chronological resolution. Quaternary Science Reviews 46, 1–29.
1096 Kohl C.P., Nishiizumi K., 1992. Chemical isolation of quartz for measurement of *in-situ* produced
1097 cosmogenic nuclides. Geochimica et Cosmochimica Acta 56, 3583–3587.
1098 Korschinek G., Bergmaier A., Faestermann T., Gerstmann U.C., Knie K., Rugel G., Wallner A.,
1099 Dillmann I., Dollinger G., von Gostomski Lierse Ch., Kossert K., Maitia M., Poutivtsev M.,
1100 Remmert A., 2009. A new value for the half-life of ^{10}Be by heavy-ion elastic recoil detection and
1101 liquid scintillation counting. Nuclear Instruments and Methods in Physics Research B 268 (2),
1102 187–191.
1103 Krivicich M., 2009. Developing the Glacial History of Middle/Lower Glacier Bay, Alaska through the
1104 Tree-Ring dating of Subfossil Wood, Glacier Bay National Park and Preserve. Undergraduate
1105 Thesis, College of Wooster, 60 pp.
1106 Kulkarni A.V., 1992. Mass balance of Himalayan glaciers using AAR and ELA methods. Journal of
1107 Glaciology 38, 101–104.
1108 Lal D., 1991. Cosmic ray labeling of erosion surfaces: in situ nuclide production rates and erosion
1109 models. Earth Planet. Sci. Lett. 104, 424–439.
1110 Larsen D.J., Miller G.H., Geirsdóttir A., Ólafsdóttir S., 2012. Non-linear Holocene climate evolution
1111 in the North Atlantic: a high-resolution, multi-proxy record of glacier activity and environmental
1112 change from Hvítárvatn, central Iceland. Quaternary Science Reviews 39, 14–25.
1113 Le Roy M., 2012. Reconstitution des fluctuations glaciaires holocènes dans les Alpes occidentales –
1114 apports de la dendrochronologie et des datations par isotopes cosmogéniques produits *in situ*. PhD
1115 Thesis, Université de Grenoble, 360 pp.
1116 Le Roy M., Deline P., 2009. Étude des fluctuations glaciaires du Petit Âge de Glace dans le Massif des
1117 Écrins: apports de la lichénometrie. Collection EDYTEM 8, 51–64.

1118 Le Roy M., Nicolussi K., Deline P., Astrade L., Edouard J-L., Miramont C., Arnaud F., 2015.
1119 Calendar-dated glacier variations in the Western European Alps during the Neoglacial: the Mer de
1120 Glace record, Mont Blanc massif. Quaternary Science Reviews 108, 1–22.
1121 Letréguilly A., Reynaud L., 1989. Past and forecast fluctuations of Glacier Blanc. Annals of
1122 Glaciology 13, 159–163.
1123 Lifton N., 2016. Implications of two Holocene time-dependent geomagnetic models for cosmogenic
1124 nuclide production rate scaling. Earth and Planetary Science Letters 433, 257–268.
1125 Lifton N., Sato T., Dunai T.J., 2014. Scaling in situ cosmogenic nuclide production rates using
1126 analytical approximations to atmospheric cosmic-ray fluxes. Earth and Planetary Science Letters
1127 386, 149–160.
1128 Luckman B.H., Masiokas M., Nicolussi K., 2017. The Neoglacial History of Robson Glacier, British
1129 Columbia. Canadian Journal of Earth Sciences, https://doi.org/10.1139/cjes-2016-0187
1130 Luetscher M., Hoffmann D.L., Frisia S., Spötl C., 2011. Holocene glacier history from alpine
1131 speleothems, Milchbach cave, Switzerland. Earth and Planetary Science Letters 302, 95–106.
1132 Luterbacher J., Werner J.P., Smerdon J.E., Fernández-Donado L., González-Rouco F.J., Barriopedro
1133 D., Ljungqvist F.C., Büntgen U., Zorita E., Wagner S., Esper J., McCarroll D., Toreti A., Frank
1134 D., Jungclaus J.H., Barriendos M., Bertolin C., Bothe O., Brázdil R., Camuffo D., Dobrovolný P.,
1135 Gagen M., García-Bustamante E., Ge Q., Gómez-Navarro J.J., Guiot J., Hao Z., Hegerl G.C.,
1136 Holmgren K., Klimenko V.V., Martín-Chivelet J., Pfister C., Roberts N., Schindler A., Schurer A.,
1137 Solomina O., von Gunten L., Wahl E., Wanner H., Wetter O., Xoplaki E., Yuan N., Zanchettin D.,
1138 Zhang H., Zerefos C., 2016. European summer temperatures since Roman times. Environmental
1139 Research Letters 11 024001.
1140 Lüthi M.P., 2014. Little Ice Age climate reconstruction from ensemble reanalysis of Alpine glacier
1141 fluctuations. Cryosphere 8, 639–650.
1142 Magny M., Bossuet G., Ruffaldi P., Leroux A., Mouthon J., 2011. Orbital imprint on Holocene
1143 palaeohydrological variations in west-central Europe as reflected by lake level changes at Cerin
1144 (Jura Mountains, eastern France). Journal of Quaternary Science 26, 2, 171–177.
1145 Magny M., Joannin S., Galop D., Vannière B., Haas J.N., Bassetti M., Bellintani P., Scandolari R.,
1146 Desmet M., 2012a. Holocene palaeohydrological changes in the northern Mediterranean
1147 borderlands as reflected by the lake-level record of Lake Ledro, northeastern Italy. Quaternary
1148 Research 77, 382–396.
1149 Magny M., Arnaud F., Billaud Y., Marquet A., 2012b. Lake-level fluctuations at Lake Bourget
1150 (eastern France) around 4500-3500 cal. BP and their palaeoclimatic and archaeological
1151 implications. Journal of Quaternary Science 27, 5, 494–502.
1152 Maisch M., Wipf A., Denneler B., Battaglia J., Benz C., 1999. Die Gletscher der Schweizer Alpen.
1153 Gletscherhochstand 1850, Aktuelle Vergletscherung, Gletscherschwund- Szenarien. Vdf
1154 Hochschulverlag ETH Zürich, 373 pp.

1155 Margreth A., Dyke A.S., Gosse J.C., Telka A.M., 2014. Neoglacial ice expansion and late Holocene
1156 cold-based ice cap dynamics on Cumberland Peninsula, Baffin Island, Arctic Canada. Quaternary
1157 Science Reviews 91, 242–256.
1158 Martin L., Blard P.-H., Balco G., Lave J., Delunel R., Lifton N., Laurent V., 2017. The CREp program
1159 and the ICE-D production rate calibration database: a fully parameterizable and updated online
1160 tool to compute cosmic-ray exposure ages. Quaternary Geochronology 38, 25–49.
1161 Marzeion B., Cogley J.G., Richter K., Parkes D., 2014. Attribution of global glacier mass loss to
1162 anthropogenic and natural causes. Science 345, 6199, 919–921.
1163 Maurer M.K., Menounos B., Luckman B.H., Osborn G., Clague J.J., Beedle M.J., Smith R., Atkinson
1164 N., 2012. Late Holocene glacier expansion in the Cariboo and northern Rocky Mountains, British
1165 Columbia, Canada. Quaternary Science Reviews 51, 71–80.
1166 McCarroll D., 2015. 'Study the past, if you would divine the future': a retrospective on measuring and
1167 understanding Quaternary climate change. Journal of Quaternary Science 30, 2, 154–187.
1168 McKay N.P., Kaufman D.S., 2009. Holocene climate and glacier variability at Hallet and Greyling
1169 Lakes, Chugach Mountains, south-central Alaska. Journal of Paleolimnology 41, 143–159.
1170 Menounos B., Clague J.J., Osborn G., Luckman B.H., Lakeman T.R., Minkus R., 2008. Western
1171 Canadian glaciers advance in concert with climate change circa 4.2 ka. Geophysical Research
1172 Letters 35, L07501, doi:10.1029/2008GL033172.
1173 Menounos B., Osborn G., Clague J.J., Luckman B.H., 2009. Latest Pleistocene and Holocene glacier
1174 fluctuations in western Canada. Quaternary Science Reviews 28, 2049–2074.
1175 Merchel S., Herpers U., 1999. An update on radiochemical separation techniques for the determination
1176 of longlived radionuclides via Accelerator Mass Spectrometry. Radiochimica Acta 84, 215–219.
1177 Miller G.H., Lehman S.J., Refsnider K.A., Southon J.R., Zhong Y., 2013. Unprecedented recent
1178 summer warmth in Arctic Canada. Geophysical Research Letters 40, 5745–5751.
1179 Millet L., Arnaud F., Heiri O., Magny M., Verneaux V., Desmet M., 2009. Late-Holocene summer
1180 temperature reconstruction from chironomid assemblages of Lake Anterne, northern French Alps.
1181 The Holocene 19, 2, 317–328.
1182 Montjuvent G., 1974. Considérations sur le relief glaciaire à propos des Alpes du Dauphiné.
1183 Geographie Physique et Géologie Dynamique 16, 465–502.
1184 Mood B.J., Smith D.J., 2015. Holocene glacier activity in the British Columbia Coast Mountains,
1185 Canada. Quaternary Science Reviews 128, 14–36.
1186 Moran A.P., Ivy Ochs S., Christl M., Kerschner H., 2017. Exposure dating of a pronounced glacier
1187 advance at the onset of the late-Holocene in the central Tyrolean Alps. The Holocene 27, 9, 1350–
1188 1358.
1189 Müller P., 1988. Parametrisierung der Gletscher-Klima-Beziehung fur die Praxis: Grundlagen und
1190 Beispiele. Mitteilungen der Versuchsanstalt für Wasserbau, Hydrologie und Glaziologie, 95, 228
1191 pp.

1192 Nicolussi K., Patzelt G., 2001. Untersuchungen zur holozänen Gletscherentwicklung von Pasterze und
1193 Gepatschferner (Ostalpen). Zeitschrift für Gletscherkunde und Glazialgeologie 36, 1–87.
1194 Nicolussi, K., Schlüchter, C., 2012. The 8.2 ka event – calendar dated glacier response in the Alps.
1195 Geology 40, 819–822.
1196 Nicolussi K., Kaufmann M., Patzelt G., van der Plicht J., Thurner A., 2005. Holocene tree-line
1197 variability in the Kauner Valley, Central Eastern Alps, indicated by dendrochronological analysis
1198 of living trees and subfossil logs. Vegetation History and Archaeobotany 14, 221–234.
1199 Nicolussi K., Jörin U., Kaiser K.F., Patzelt G., Thurner A., 2006. Precisely dated glacier fluctuations
1200 in the Alps over the last four millennia. In: Price, M.F. (Ed.), Global Change in Mountain Regions.
1201 Sapiens Publishing, pp. 59–60.
1202 Nicolussi K., Kauffmann M., Melvin T.M., Van Der Plicht J., Schiessling P., Thurner A., 2009. A
1203 9111 year long conifer tree ring chronology for the European Alps: a base for environmental and
1204 climatic investigations. The Holocene 19, 6, 909–920.
1205 Nicolussi K., Matuschik I., Tegel W., 2013. Klimavariabilität und Siedlungsdynamik am Beispiel der
1206 Feuchtbodensiedlungen im Raum Oberschwaben, Bodensee und Nordostschweiz 4400-3400 BC.
1207 In: Bleicher N., Schlichtherle H., Gassmann P., Martinelli N. (Eds), Dendro – Chronologie –
1208 Typologie – Ökologie. Festschrift für André Billamboz zum 65. Geburtstag. Freiburg i. Br., 61–
1209 77.
1210 Nishiizumi K., Imamura M., Caffee M.W., Southon J.R., Finkel R.C., McAninch J., 2007. Absolute
1211 calibration of ^{10}Be AMS standards. Nuclear Instruments and Methods in Physics Research B 258,
1212 403–413.
1213 N.O.A.A., 1976. U.S. Standard Atmosphere. US Gov. Print. Off.
1214 Oerlemans J., 2005. Extracting a climate signal from 169 glacier records. Science 308, 675–677.
1215 O'Neal M.A., 2006. The effects of slope degradation on lichenometric dating of Little Ice Age
1216 moraines. Quaternary Geochronology 1, 121–128.
1217 Orombelli G., 1998. Le torbe del Rutor: una successione significativa per la storia olocenica dei
1218 ghiacciai e del clima nelle alpi. Memorie della Società Geografica Italiana 55, 153–165.
1219 Osborn G., Menounos B., Ryane C., Riedel J., Clague J.J., Koch J., Clark D., Scott K., Davis P.T.,
1220 2012. Latest Pleistocene and Holocene glacier fluctuations on Mount Baker, Washington.
1221 Quaternary Science Reviews 49, 33–51.
1222 Osborn G., Haspel R., Spooner I., 2013. Late-Holocene fluctuations of the Bear River Glacier,
1223 northern Coast Ranges of British Columbia, Canada. The Holocene 23, 3, 330–338.
1224 Patzelt G., 1974. Holocene variations of glaciers in the Alps. Colloques Internationaux du CNRS,
1225 n°219 – Les méthodes quantitatives d'étude des variations du climat au cours du Pleistocène, 51–
1226 59.
1227 Patzelt G., 1985. Glacier advances in the Alps 1965 to 1980. Zeitschrift für Gletscherkunde und
1228 Glazialgeologie 21, 403–407.

1229 Patzelt G., 1995. Die klimatischen Verhältnisse im südlichen Mitteleuropa zur Römerzeit. In: Bender
1230 H. & Wolff H. (Eds.): Ländliche Besiedlung und Landwirtschaft in den Rhein-Donau-Provinzen
1231 in der römischen Kaiserzeit. Passauer Universitätsschriften zur Archäologie 2, 7–20.
1232 Patzelt G., Bortenschlager S., 1973. Die postglazialen Gletscher- und Klimaschwankungen in der
1233 Venedigergruppe (Hohe Tauern, Ostalpen). Zeitschrift für Geomorphologie N.F. Suppl. band 16,
1234 25–72.
1235 Paul F., Frey H., Le Bris R., 2011. A new glacier inventory for the European Alps from Landsat TM
1236 scenes of 2003: challenges and results. Annals of Glaciology 52, 59, 144–152.
1237 Pech P., Jomelli V., Baumgart-Kotarba M., Bravard J.-P., Chardon M., Jacob N., Kedzia S., Kotarba
1238 A., Raczkowska Z., Tsao C., 2003. A lichenometric growth curve in the French Alps: Ailefroide
1239 and Veneon valleys; Massifs des Ecrins. Geodinamica Acta 16, 187–193.
1240 Pelfini M., Leonelli G., Trombino L., Zerboni A., Bollati I., Merlini A., Smiraglia C., Diolaiuti G.,
1241 2014. New data on glacier fluctuations during the climatic transition at ~4,000 cal. year BP from a
1242 buried log in the Forni Glacier forefield (Italian Alps). Rendiconti Lincei 25, 427–437.
1243 Pellitero R., Rea B.R., Spagnolo M., Bakke J., Hughes P., Ivy-Ochs S., Lukas S., Ribolini A., 2015. A
1244 GIS tool for automatic calculation of glacier equilibrium-line altitudes. Computers & Geosciences
1245 82, 55–62.
1246 Pindur P., Heuberger H., 2010. Zur holozänen Gletschergeschichte im Zemmgrund in den Zillertaler
1247 Alpen, Tirol (Ostalpen). Zeitschrift für Gletscherkunde und Glazialgeologie 42, 21–89.
1248 Putkonen J., O'Neal M., 2006. Degradation of unconsolidated Quaternary landforms in the western
1249 North America. Geomorphology 75, 408–419.
1250 Putkonen J., Connolly J., Orloff T., 2008. Landscape evolution degrades the geologic signature of past
1251 glaciations. Geomorphology 97, 208–217.
1252 Putnam A.E., Schaefer J.M., Denton G.H., Barrell D.J.A., Finkel R.C., Andersen B.G., Schwartz R.,
1253 Chinn T.J.H., Doughty A.M., 2012. Regional climate control of glaciers in New Zealand and
1254 Europe during the pre-industrial Holocene. Nature Geoscience 5, 627–630.
1255 Rabatel A., Dedieu J.P., Thibert E., Letréguilly A., Vincent C., 2008. 25 years (1981–2005) of
1256 equilibrium-line altitude and mass-balance reconstruction on Glacier Blanc, French Alps, using
1257 remote-sensing methods and meteorological data. Journal of Glaciology 54, 185, 307–314.
1258 Rabatel A., Letréguilly A., Dedieu J.-P., Eckert N., 2013. Changes in glacier equilibrium-line altitude
1259 in the western Alps from 1984 to 2010: evaluation by remote sensing and modeling of the
1260 morpho-topographic and climate controls. Cryosphere 7, 1455–1471.
1261 Rabatel A., Dedieu J.P., Vincent C., 2016. Spatio-temporal changes in glacier-wide mass balance
1262 quantified by optical remote sensing on 30 glaciers in the French Alps for the period 1983–2014.
1263 Journal of Glaciology 62, 236, 1153–1166.
1264 Rea B.R. 2009. Defining modern day Area-Altitude Balance Ratio (AABRs) and their use in glacier-
1265 climate reconstructions. Quaternary Science Reviews 28, 237–248.

1266 Reimer P.J., Bard E., Bayliss A., Beck J.W., Blackwell P.J., Bronk Ramsey C., Buck C.E., Cheng H.,
1267 Edwards R.L., Friedrich M., Grootes P.M., Guilderson T.P., Haflidason H., Hajdas I., Hatté C.,
1268 Heaton T.J., Hoffmann D.L., Hogg A.G., Hughen K.A., Kaiser K.F., Kromer B., Manning S.W.,
1269 Niu M., Reimer R.W., Richards D.A., Scott E.M., Southon J.R., Staff R.A., Turney C.S.M., van
1270 der Plicht J., 2013. IntCal13 and MARINE13 radiocarbon age calibration curves 0-50,000 years
1271 cal BP. Radiocarbon 55, 4, 1869–1887.
1272 Renner F., 1982. Beiträge zur Gletschergeschichte des Gottardgebietes und dendroklimatologische
1273 Analysen an fossilen Hölzern. Physische Geographie 8. Zürich.
1274 Reynaud L., 1998. Suivis glaciologiques dans les Ecrins 1997, rapport au Parc National des Ecrins. 36
1275 pp.
1276 Reynaud L., Vincent C., 2000. Relevés de fluctuations sur quelques glaciers français. La Houille
1277 Blanche 5, 79–86.
1278 RinnTech, 2005. TSAP-Win. Time Series Analysis and Presentation for Dendrochronology and
1279 Related Application. Version 0.53. www.rinntech.com.
1280 Roe G.H., Baker M.B., Herla F., 2017. Centennial glacier retreat as categorical evidence of regional
1281 climate change. Nature Geoscience 10, 95–99.
1282 Sass-Klaassen U., Hanraets E., 2006. Woodlands of the past - The excavation of wetland woods at
1283 Zwolle-Stadshagen (the Netherlands), Growth pattern and population dynamics of oak and ash.
1284 Netherlands Journal of Geosciences 85, 1, 61–71.
1285 Scherler D., Bookhagen B., Strecker M.R., 2011. Hillslope-glacier coupling: the interplay of
1286 topography and glacial dynamics in High Asia, J. Geophys. Res., 116, F02019,
1287 doi:10.1029/2010JF001751.
1288 Schildgen T.F., Phillips W.M., Purves R.S., 2005. Simulation of snow shielding corrections for
1289 cosmogenic nuclide surface exposure studies. Geomorphology 64, 67–85.
1290 Schimmelpfennig I., Schaefer J.M., Akçar N., Ivy-Ochs S., Finkel R.C., Schlüchter C., 2012.
1291 Holocene glacier culminations in the Western Alps and their hemispheric relevance. Geology 40,
1292 891–894.
1293 Schimmelpfennig I., Schaefer J.M., Akçar N., Koffman T., Ivy-Ochs S., Schwartz R., Finkel R.C.,
1294 Zimmerman S., Schlüchter C.A., 2014. Chronology of Holocene and Little Ice Age glacier
1295 culminations of the Steingletscher, Central Alps, Switzerland, based on high-sensitivity beryllium-
1296 10 moraine dating. Earth Planet. Sci. Lett. 393, 220–230.
1297 Schmidt G.A., Annan J.D., Bartlein P.J., Cook B.I., Guilyardi E., Hargreaves J.C., Harrison S.P.,
1298 Kageyama M., LeGrande A.N., Konecky B., Lovejoy S., Mann M.E., Masson-Delmotte V., Risi
1299 C., Thompson D., Timmermann A., Tremblay L.B., Yiou P., 2014. Using palaeo-climate
1300 comparisons to constrain future projections in CMIP5. Climate of the Past 10, 221–250.
1301 Schneebeli W., 1976. Untersuchungen von Gletscherschwankungen im Val de Bagnes. Die Alpen 52,
1302 5–57.

1303 Schweinsberg A.D., Briner J.P., Miller G.H., Bennike O., Thomas E.K., 2017. Local glaciation in
1304 West Greenland linked to North Atlantic Ocean circulation during the Holocene. Geology 45, 3,
1305 195–198.
1306 Sigl M., Winstrup M., McConnell J.R., Welten K.C., Plunkett G., Ludlow F., Büntgen U., Caffee M.,
1307 Chellman N., Dahl-Jensen D., Fischer H., Kipfstuhl S., Kostick C., Maselli O.J., Mekhaldi F.,
1308 Mulvaney R., Muscheler R., Pasteris D.R., Pilcher J.R., Salzer M., Schüpbach S., Steffensen J.P.,
1309 Vinther B.M., Woodruff T.E., 2015. Timing and climate forcing of volcanic eruptions for the past
1310 2,500 years. Nature 523, 543–549.
1311 Sigl M., Osmont D., Gabrieli J., Barbante C., Schwikowski M., 2016. End of the 'Little Ice Age' in
1312 the Alps not forced by industrial black carbon. Geophysical Research Abstracts Vol. 18,
1313 EGU2016-14585, 2016.
1314 Sissons J.B., 1977. The Loch Lomond Advance in the Northern Mainland of Scotland. In: Gray, J.M.,
1315 Lowe, J.J. (Eds.), Studies in the Scottish Lateglacial Environment. Pergamon Press, Oxford, 45–
1316 59.
1317 Six D., Vincent C., 2014. Sensitivity of mass balance and equilibrium-line altitude to climate change
1318 in the French Alps. Journal of Glaciology 60, 223, 867–878.
1319 Small D., Fabel D., 2015. A Lateglacial ^{10}Be production rate from glacial lake shorelines in Scotland.
1320 Journal of Quaternary Science 30, 6, 509–513.
1321 Solomina O.N., Bradley R.S., Hodgson D.A., Ivy-Ochs S., Jomelli V., Mackintosh A.N., Nesje A.,
1322 Owen L.A., Wanner H., Wiles G.C., Young N.E., 2015. Holocene glacier fluctuations. Quaternary
1323 Science Reviews 111, 9–34.
1324 Solomina O.N., Bradley R.S., Jomelli V., Geirsdottir A., Kaufman D.S., Koch J., McKay N.P.,
1325 Masiokas M., Miller G., Nesje A., Nicolussi K., Owen L.A., Putnam A.E., Wanner H., Wiles G.,
1326 Yang B., 2016. Glacier fluctuations during the past 2000 years. Quaternary Science Reviews 149,
1327 61–90.
1328 Stone J.O., 2000. Air pressure and cosmogenic isotope production. J. Geophys. Res. 105, 23753.
1329 Striberger J., Björck S., Holmgren S., Hamerlík L., 2012. The sediments of Lake Lögurinn – A unique
1330 proxy record of Holocene glacial meltwater variability in eastern Iceland. Quaternary Science
1331 Reviews 38, 76–88.
1332 Stroeven A.P., Heyman J., Fabel D., Björck S., Caffee M.W., Fredin O., Harbor J.M., 2015. A new
1333 Scandinavian reference ^{10}Be production rate. Quaternary Geochronology 29, 104–115.
1334 Stuiver M., Reimer P.J., Reimer R.W., 2017. CALIB 7.1 [WWW program] at http://calib.org.
1335 Telford R.J., Heegaard E., Birks H.J.B., 2004. The intercept is a poor estimate of a calibrated
1336 radiocarbon age. The Holocene 14, 296–298.
1337 Tessier L., Coûteaux M., Guiot J., 1986. An attempt at an absolute dating of a sediment from the last
1338 glacial recurrence through correlations between pollen analytical and tree-ring data. Pollen et
1339 Spores 28, 61–76.

Thibert E., Faure J., Vincent C., 2005. Bilans de masse du Glacier Blanc entre 1952, 1981 et 2002 obtenus par modèles numériques de terrain. La Houille Blanche 2, 72–78.

Toohey M., Krüger K., Sigl M., Stordal F., Svensen H., 2016. Climatic and societal impacts of a volcanic double event at the dawn of the Middle Ages. Climatic Change 136, 3, 401–412.

Uppala S.M., Kållberg P., Simmons A., Andrae U., Bechtold V., Fiorino M., Gibson J., Haseler J., Hernandez A., Kelly G.A., Li X., Onogi K., Saarinen S., Sokka N., Allan R.P., Andersson E., Arpe K., Balmaseda M.A., Beljaars A.C.M., Berg L. Van De, Bidlot J., Bormann N., Caires S., Chevallier F., Dethof A., Dragosavac M., Fisher M., Fuentes M., Hagemann S., Hólm E., Hoskins B.J., Isaksen L., Janssen P.A.E.M., Jenne R., McNally A.P., Mahfouf J.-F., Morcrette J.-J., Rayner N.A., Saunders R.W., Simon P., Sterl A., Trenberth K.E., Untch A., Vasiljevic D., Viterbo P., Woollen J., 2005. The ERA-40 reanalysis. Quarterly Journal of the Royal Meteorological Society 131, 2961–3012.

Valla P.G, van der Beek P.A., Lague D., 2010. Fluvial incision into bedrock: Insights from morphometric analysis and numerical modeling of gorges incising glacial hanging valleys (Western Alps, France). Journal of Geophysical Research 115, F02010, doi:10.1029/2008JF001079.

van der Beek P., Bourbon P., 2008. A quantification of the glacial imprint on relief development in the French Western Alps. Geomorphology 97, 52–72.

van der Bilt W.G., Bakke J., Vasskog K., D'Andrea W.J., Bradley R.S., Ólafsdóttir S., 2015. Reconstruction of glacier variability from lake sediments reveals dynamic Holocene climate in Svalbard. Quaternary Science Reviews 126, 201–218.

Vasskog K., Paasche Ø, Nesje A., Boyle J.F., Birks H.J.B., 2012. A new approach for reconstructing glacier variability based on lake sediments recording input from more than one glacier. Quaternary Research 77, 192–204.

Vincent C., Le Meur E., Six D., 2005. Solving the paradox of the end of the Little Ice Age in the Alps. Geophysical Research Letters 32, L09706, doi:10.1029/2005GL022552.

Vincent C., Fischer A., Mayer C., Bauder A., Galos S.P., Funk M., Thibert E., Six D., Braun L., Huss M., 2017. Common climatic signal from glaciers in the European Alps over the last 50 years. Geophysical Research Letters 44, 1376–1383, doi:10.1002/2016GL072094.

Vivian R., 1979. Les glaciers sont vivants. Denoël, 240 pp.

Von Blanckenburg F., Belshaw N.S., O'Nions R.K., 1996. Separation of ^{9}Be and cosmogenic ^{10}Be from environmental materials and SIMS isotope dilution analysis. Chemical Geology 129, 1-2, 93–99.

Walker M.J.C., Berkelhammer M., Björck S., Cwynar L.C., Fisher D.A., Long A.J., Lowe J.J., Newnham R.M., Rasmussen S.O., Weiss H., 2012. Formal subdivision of the Holocene Series/Epoch: a Discussion Paper by a Working Group of INTIMATE (Integration of ice-core,

marine and terrestrial records) and the Subcommission on Quaternary Stratigraphy (International Commission on Stratigraphy). Journal of Quaternary Science 27, 7, 649–659.

Wanner H., Solomina O., Grosjean M., Ritz S.P., Jetel M., 2011. Structure and origin of Holocene cold events. Quaternary Science Reviews 30, 3109-3123.

Wäspi H., 1993. Zur Glazialmorphologie und Gletschergeschichte des Gauli (Grimselgebiet, Kt. Bern). Diploma Thesis, Geographisches Institut der Universität Zürich, 130 pp.

Wiles G.C., Barclay D.J., Young N.E., 2010. A review of lichenometric dating of glacial moraines in Alaska. Geografiska Annaler 92 A, 1, 101–109.

Winkler S., Chinn T., Gärtner-Roer I., Nussbaumer S.U., Zemp, M., Zumbühl, H.J., 2010. An introduction to mountain glaciers as climate indicators with spatial and temporal diversity. Erdkunde 64, 2, 97–118.

Wipf A., 2001. Gletschergeschichtliche Untersuchungen im Spät- und Postglazialen Bereich des Hinteren Lauterbrunnentals (Berner Oberland, Schweiz). Geographica Helvetica 56, 2, 133–144.

Young N.E., Briner J.P., Kaufman D.S., 2009. Late Pleistocene and Holocene glaciation of the Fish Lake valley, northeastern Alaska Range, Alaska. Journal of Quaternary Science 24, 677–689.

Young N.E., Schaefer J.M., Briner J.P., Goehring B.M., 2013. A ^{10}Be production rate calibration for the Arctic. Journal Quaternary Science 28, 515–526.

Young N.E., Schweinsberg A.D., Briner J.P., Schaefer J.M., 2015. Glacier maxima in Baffin Bay during the Medieval Warm Period coeval with Norse settlement. Science Advances 1, 11. e1500806.

Zerathe S., Lebourg T., Braucher R., Bourlès D., 2014. Mid-Holocene cluster of large-scale landslides revealed in the Southwestern Alps by ^{36}Cl dating. Insight on an Alpine-scale landslide activity. Quaternary Science Reviews 90, 106–127.

Zoller H., Schindler C., Röthlisberger H., 1966. Postglaziale Gletscherstände und Klimaschwankungen im Gotthardmassiv und Vorderrheingebiet. Verh. Naturforsch. Ges. Basel 77, 97–164.

Zumbühl H.J., Holzhauser H., 1988. Alpengletscher in der Kleinen Eiszeit. Die Alpen 64, 3, 129–322.

Fig. 1. (a) Location of the Ecrins-Pelvoux Massif (EPM) in the Alps. White areas: AD 2003 glacier extent (**Paul et al., 2011**). Glaciers (black font) and other locations (grey font) cited in the text are indicated ('Schwarz.' stands for Schwarzenstein Glacier). Western Alps glacierized massifs are shown with outlined font, MBM: Mont Blanc Massif, VA: Vanoise, BLD: Belledonne, GR: Grandes Rousses, UB: Ubaye, MA: Maritime Alps. Lower right inset: location of the Alps in Europe; **(b)** Shaded-relief map of the EPM with Little Ice Age (LIA) and present day (AD 2009) glacier extents (**Gardent et al., 2014**). Study sites are highlighted in red, and other EPM glaciers (5 to 7) and lakes cited in the text are indicated. The digital elevation model is an extract of the BD ALTI database from IGN (Institut national de l'information géographique et forestière). Eastings and northings are according to the IGN Lambert 93 grid in km.

Fig. 2. Geomorphological maps of the four study sites. **(a)** Rateau Glacier; **(b)** Lautaret Glacier; **(c)** Bonnepierre Glacier; **(d)** Etages Glacier. Contour interval is 50 m. Eastings and northings are according to the IGN Lambert 93 grid in m.

Fig. 3. ^{10}Be moraine boulder dating results. Exposure ages (yellow boxes) are reported as ka before AD 2000 rounded to the nearest decade and are grouped by moraine ridge. Errors are 1 σ internal uncertainties (analytical errors only). **(a)** Rateau Glacier moraines MA to MD; **(b)** Lautaret Glacier moraine MA ; **(c)** Bonnepierre Glacier moraines MA to ME; **(d)** Etages Glacier moraine M1. Orange box is the dendro-date of subfossil log eta01. Purple boxes show apparent ages derived from glaciogenic material (sands and gravels) collected by **Delunel et al (2014a)**. Etages Glacier map is not at the same scale. Eastings and northings are according to the IGN Lambert 93 grid in m.

Fig. 4. Field photographs summarizing moraine ages determined in this study (see **Fig. 3** for location of shooting places). Reported errors include PR uncertainty; **(a)** Rateau Glacier sampled ridges MA to MD. Ages indicated for MA to MC are 'apparent ages' based on the oldest boulder age per moraine (rather than mean ages) owing to discordant results at this site (see main text). Age for MD, also based on a single boulder, is thought to be the most reliable at this site (see main text). Non-sampled ridges MF to MH are also shown (ridge ME is obscured); **(b)** Lautaret Glacier composite left lateral moraine (left image). Sampled ridge MA is cross-cut by immediately inboard ridge MB. Right image: close-up of boulder LAU01 on moraine MA with sample location (white arrow). Notebook (30 cm-long) for scale; **(c)**

Bonnepierre Glacier sampled ridges MA to ME with mean ages. No mean age was computed for MD as only outliers were identified on this ridge. Moraine MC and MD are obscured; **(d)** Etages Glacier frontal ridges M1 to M6 and mean age for ridge M1 (left image). Red arrow: avalanche path; orange circle: sampling location of the subfossil detrital log eta01. Right image: close-up of moraine M1 with sampled boulders (white arrows).

Fig. 5. Eta01 subfossil log indexed tree-ring series (67 % spline) along with crossdating results computed with TSAP-Win software (**Rinntech, 2005**) on two distant references: the Eastern Alpine Conifer Chronology (**Nicolussi et al., 2009**) in red and the Mont Blanc massif chronology (**Le Roy et al., 2015**) in purple. Light blue intervals highlight periods of depressed growth. The close-up photograph of the wood section shows the eccentric growth pattern of this tree.

Fig. 6. Holocene paleoclimate proxies for the Alps. The period of rapid climate change between 4.4 and 4.0 ka, proposed as marking the onset of the Neoglacial period, is highlighted (light blue shading). **(a)** COMNISPA II, speleothem $\delta^{18}O$ composite record from Spannagel Cave (2340 m a.s.l.; western Austrian Alps; **Fohlmeister et al., 2013**); **(b)** Treeline variations in the Kauner Valley (western Austrian Alps; **Nicolussi et al., 2005**); **(c)** Radiocarbon and dendrochronological dating indicating smaller-than-present (AD 1990-2010) glacier extent in the Swiss and Austrian Alps (**Nicolussi and Patzelt, 2001**; **Joerin et al., 2006**; **2008**; **Drescher-Schneider and Kellerer-Pirklhauer 2008**; **Nicolussi and Schlüchter 2012**). Data falling into the 4.4-4.0 ka interval come only from the slow reacting Unteraar Glacier; **(d)** Advances of Gepatsch Glacier (western Austrian Alps) similar to – or beyond – its AD 1960 extent (**Nicolussi and Patzelt, 2001**); **(e)** Radiocarbon dating carried on subfossil soils and woods, indicating Holocene glacier maxima in the Swiss Alps (**Furrer et al., 1987**); **(f)** Upper Grindelwald Glacier (Bernese Swiss Alps) tongue elevation reconstructed from speleothem fabrics (**Luetscher et al., 2011**); **(g)** Summed Gaussian probability curves of TCN-dated Neoglacial moraines in the Ecrins-Pelvoux massif (this work). Thin white lines are individual boulder probability curves generated with external uncertainties (including PR uncertainty). Dotted thin lines represent outliers ages not included in moraine age calculation. Rateau Glacier dating are not displayed here, except moraine MD, because of discordant results (see main text). Summed curve for the LAP include mean ages of Bonnepierre Glacier moraines MB and MC and Rateau Glacier moraine MD (three moraines); **(h)** Terrigenous input into sub-alpine Lake Bourget (northern French Prealps; **Arnaud et al., 2012**); **(i)** Ledro

lake-level record (northern Italy; **Magny et al., 2012a**); **(j)** Cerin lake-level record (French Jura Mountains; **Magny et al., 2011**).

Fig. 7. Comparison of the timing of Neoglacial advances in the Ecrins-Pelvoux massif with selected proxies of glacial activity in the western Alps. **(a)** Sample depth of the dendro-dated subfossil trees retrieved from the Mer de Glace right lateral moraine (Mont Blanc massif; **Le Roy et al., 2015,** supplemented). Replication peaks are interpreted as reflecting Neoglacial interstadial conditions and abrupt dying-off phases are interpreted as burial events caused by glacier advances; **(b)** Summed probability distribution of the calibrated radiocarbon dates from archaeological artefacts found at Schnidejoch Pass (2756 m a.s.l., Bernese Swiss Alps; **Hafner and Schwörer, 2017**) generated with Oxcal 4.3 (**Bronk Ramsey and Lee, 2013**). This dataset is thought to reflect contraction periods of the neighbouring Chilchli Glacier, allowing easier traverse of the pass; **(c)** Summed Gaussian probability curves of TCN-dated Neoglacial moraines in the EPM (this work). Thin white lines are individual boulder probability curves generated with external uncertainties (including PR uncertainty). Dotted thin lines represent outliers ages not included in moraine age calculation. Rateau Glacier dating are not displayed here, except moraine MD, because of discordant results (see main text). LAP: Löbben Advance Period; GII: Göschenen 2; HMA: High Medieval Advance. Summed curve for the LAP include mean ages of Bonnepierre Glacier moraines MB and MC and Rateau Glacier moraine MD (three moraines). Vertical dashed lines are moraine mean ages; **(d)** Proglacial Lake Muzelle clastic sedimentation (**Fouinat et al., 2017**; **Fig. 1b**) based on the RABD (I-band) reflectance spectroscopy index (**Boldt et al., 2015**); **(e)** Proglacial Lake Bramant clastic sedimentation (2448 m a.s.l., Grandes Rousses massif; **Fig. 1a**). K/Ti anomalies are shown up to 800 AD (left axis); Ti anomalies are shown from 800 AD onwards (right axis). Both anomalies are considered proxies for the Saint Sorlin Glacier activity during these two time periods (**Guyard et al., 2013**).

Tab. 1. Basic topographic characteristics of the studied glaciers. Neoglacial and current (AD 2009) glacier surface data are taken from **Gardent et al. (2014)**.

[a] Neoglacial extent is considered to be similar to LIA extent (see main text)

[b] Numbers in brackets represent the total area of the presently separated ice bodies that were connected during the Neoglacial maxima.

[c] Current average slope is the weighted mean slope for these bodies (except for Rateau Glacier).

[d] Debris-covered tongue is now separated from the main glacier body.

[e] Calculated with an Accumulation Area Ratio (AAR) of 0.67 (0.4 for Bonnepierre Glacier) and 10 m contour interval.

[f] Calculated with an Area Altitude Balance Ratio (AABR) of 1.6 (0.9 for Bonnepierre Glacier) and 10 m contour interval.

Tab. 2. ^{10}Be sample characteristics.

[a] Rateau Glacier sample heights above the ground are the average of four point measurement per boulder (along and perpendicular to the long axis).

Tab. 3. ^{10}Be sample exposure ages.

[a] ^{10}Be/^{9}Be ratios of batch-specific analytical blanks used for the correction are $(1.4 \pm 0.8) \times 10^{-15}$ and $(2.0 \pm 1.0) \times 10^{-15}$ for samples marked with (†), $(2.0 \pm 0.9) \times 10^{-15}$ for samples marked with (‡), $(2.8 \pm 1.3) \times 10^{-15}$, $(2.5 \pm 1.1) \times 10^{-15}$ and $(2.7 \pm 1.2) \times 10^{-15}$ for samples marked with (§) and $(9.7 \pm 1.3) \times 10^{-15}$ for samples marked with (#). When multiple blanks have been processed within a single batch, mean value was used for the correction.

[b] Age calculations use density values of 2.54 and 2.62 g cm^3 for granite and gneiss, respectively (**Delunel, 2010**) and zero erosion. 'LSD/Chironico' exposure ages are calculated with the CREp program (**Martin et al., 2017**) using the LSD scaling model (**Lifton et al., 2014**) and the Chironico landslide production rate (**Claude et al., 2014**). 'Lm/Arctic' exposure ages are calculated with the CRONUS-Earth online calculator (version 2.2; **Balco et al., 2008**) using the time-dependent Lal/Stone scaling model (**Lal, 1991**; **Stone, 2000**) and the 'Arctic' production rate (**Young et al., 2013**).

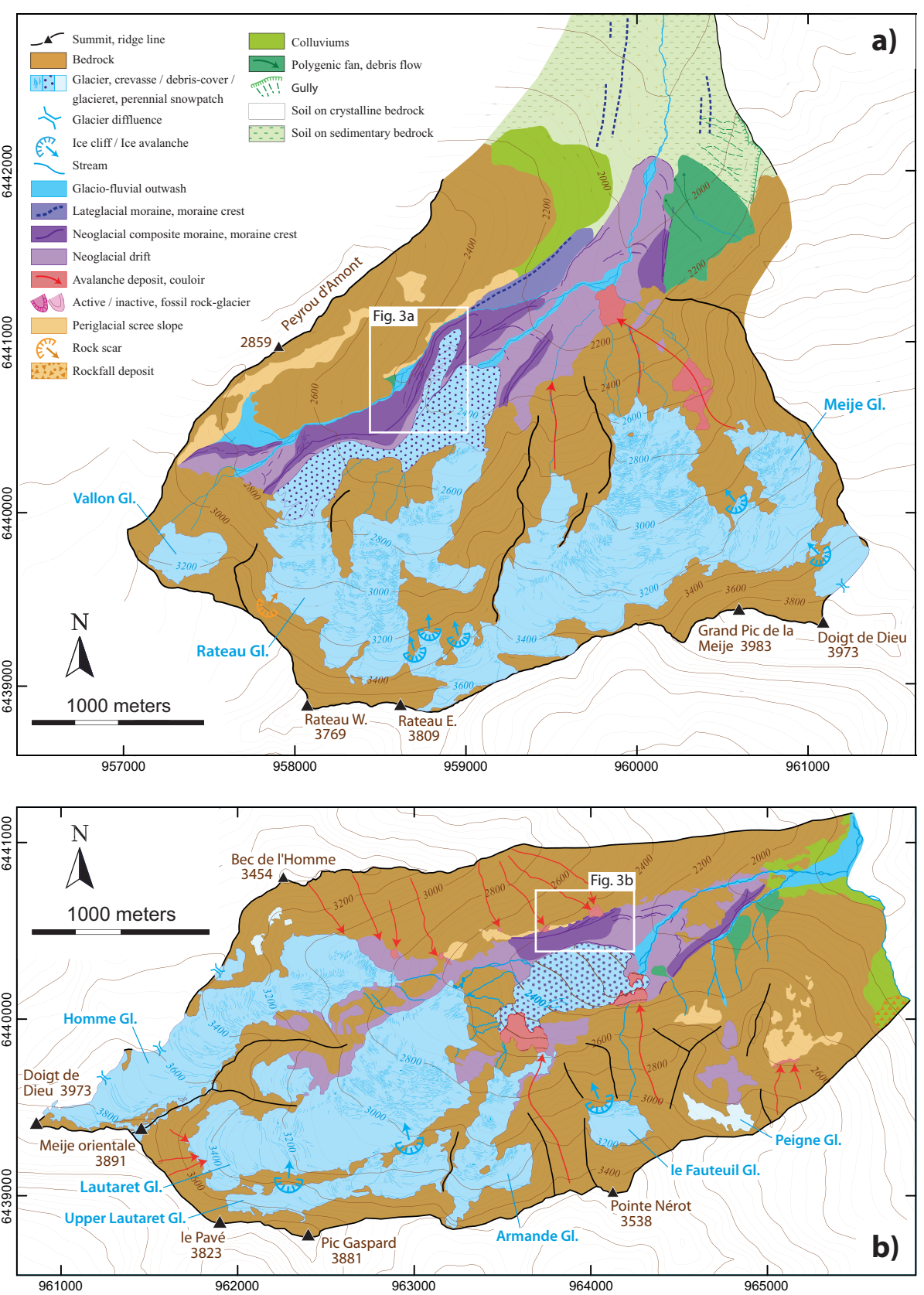
a)
Summit, ridge line
Bedrock
Glacier, crevasse / debris-cover / glacieret, perennial snowpatch
Glacier diffluence
Ice cliff / Ice avalanche
Stream
Glacio-fluvial outwash
Lateglacial moraine, moraine crest
Neoglacial composite moraine, moraine crest
Neoglacial drift
Avalanche deposit, couloir
Active / inactive, fossil rock-glacier
Periglacial scree slope
Rock scar
Rockfall deposit
Colluviums
Polygenic fan, debris flow
Gully
Soil on crystalline bedrock
Soil on sedimentary bedrock
Peyrou d'Amont
2859
Fig. 3a
Meije Gl.
Vallon Gl.
Rateau Gl.
Grand Pic de la Meije 3983
Doigt de Dieu 3973
Rateau W. 3769
Rateau E. 3809
N
1000 meters
6442000
6441000
6440000
6439000
957000
958000
959000
960000
961000
b)
Bec de l'Homme 3454
Fig. 3b
Homme Gl.
Doigt de Dieu 3973
Meije orientale 3891
Lautaret Gl.
Upper Lautaret Gl.
le Pavé 3823
Pic Gaspard 3881
Armande Gl.
Pointe Nérot 3538
le Fauteuil Gl.
Peigne Gl.
N
1000 meters
6441000
6440000
6439000
961000
962000
963000
964000
965000

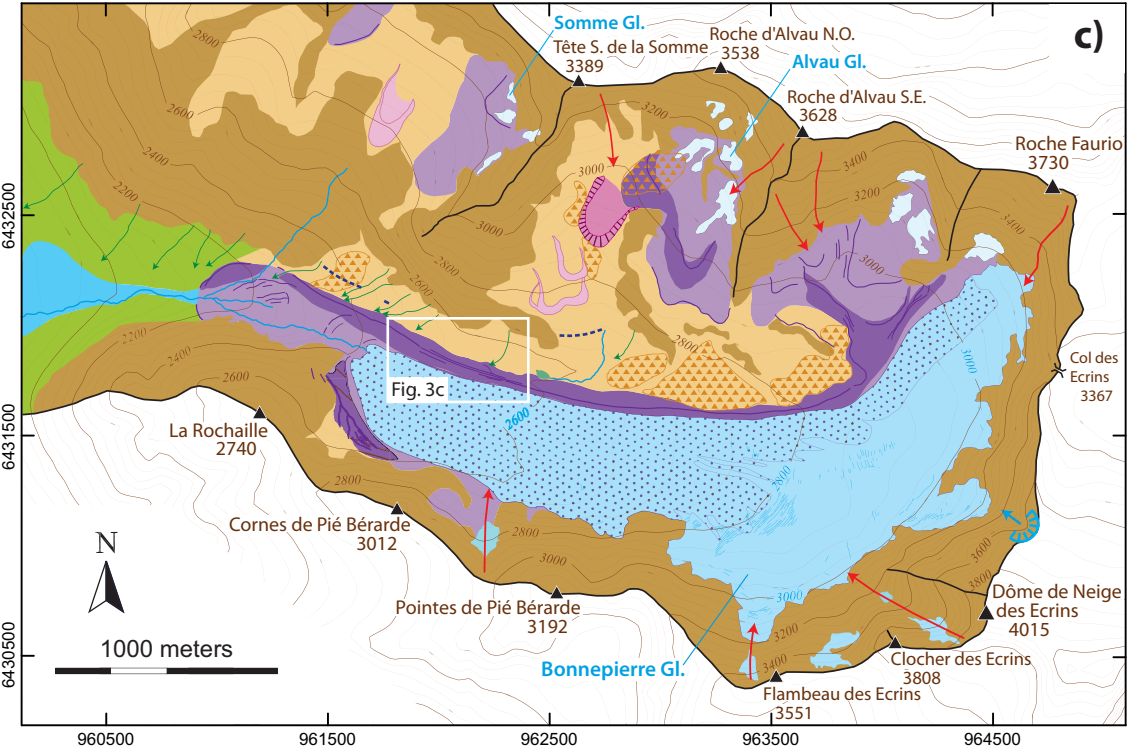
c)
Somme Gl.
Tête S. de la Somme
3389
Roche d'Alvau N.O.
3538
Alvau Gl.
Roche d'Alvau S.E.
3628
Roche Faurio
3730
Col des
Ecrins
3367
Fig. 3c
La Rochaille
2740
Cornes de Pié Bérarde
3012
Pointes de Pié Bérarde
3192
Bonnepierre Gl.
Dôme de Neige
des Ecrins
4015
Clocher des Ecrins
3808
Flambeau des Ecrins
3551
N
1000 meters
6432500
6431500
6430500
960500
961500
962500
963500
964500

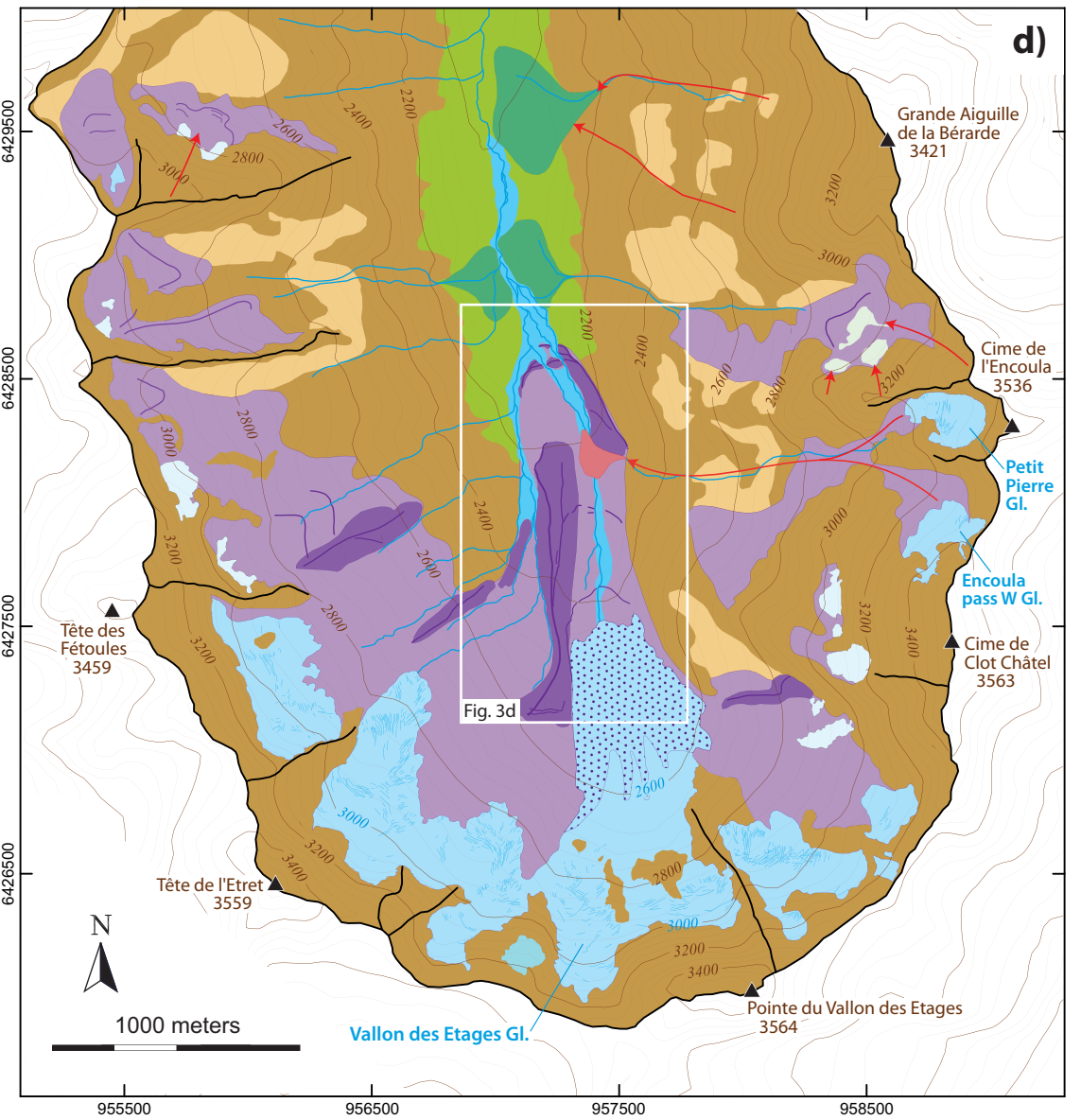
d)
Grande Aiguille
de la Bérarde
3421
Cime de
l'Encoula
3536
Petit
Pierre
Gl.
Encoula
pass W Gl.
Cime de
Clot Châtel
3563
Tête des
Fétoules
3459
Fig. 3d
Tête de l'Etret
3559
Pointe du Vallon des Etages
3564
Vallon des Etages Gl.
N
1000 meters
6429500
6428500
6427500
6426500
955500
956500
957500
958500

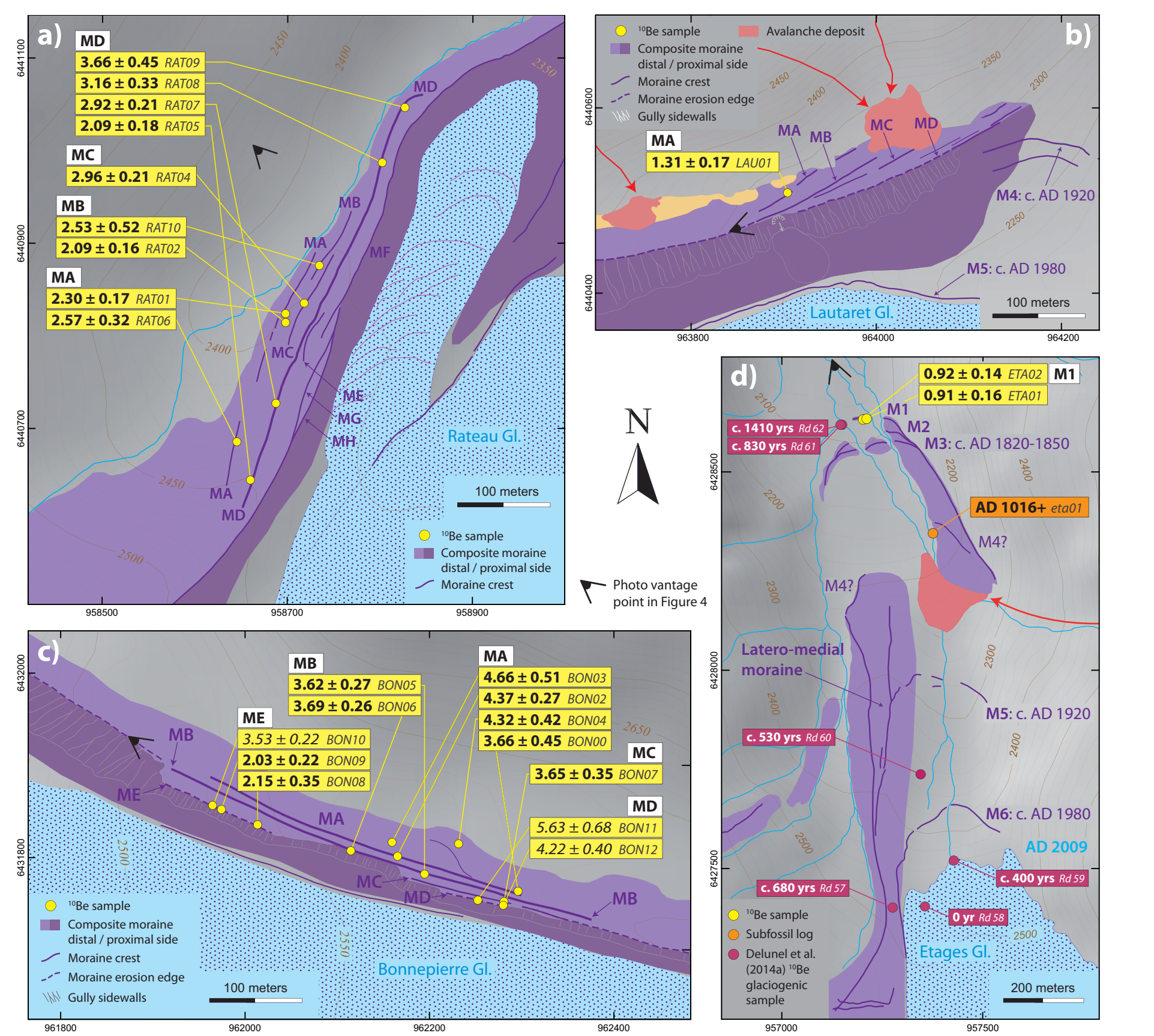
a)
MD
3.66 ± 0.45 RAT09
3.16 ± 0.33 RAT08
2.92 ± 0.21 RAT07
2.09 ± 0.18 RAT05
MC
2.96 ± 0.21 RAT04
MB
2.53 ± 0.52 RAT10
2.09 ± 0.16 RAT02
MA
2.30 ± 0.17 RAT01
2.57 ± 0.32 RAT06
MF
ME
MG
MH
Rateau Gl.
100 meters
10Be sample
Composite moraine distal / proximal side
Moraine crest
6441100
6440900
6440700
958500
958700
958900
b)
10Be sample
Avalanche deposit
Composite moraine distal / proximal side
Moraine crest
Moraine erosion edge
Gully sidewalls
MA
1.31 ± 0.17 LAU01
MB
MC
MD
M4: c. AD 1920
M5: c. AD 1980
Lautaret Gl.
100 meters
6440600
6440400
963800
964000
964200
N
Photo vantage point in Figure 4
c)
MB
3.62 ± 0.27 BON05
3.69 ± 0.26 BON06
ME
3.53 ± 0.22 BON10
2.03 ± 0.22 BON09
2.15 ± 0.35 BON08
MA
4.66 ± 0.51 BON03
4.37 ± 0.27 BON02
4.32 ± 0.42 BON04
3.66 ± 0.45 BON00
MC
3.65 ± 0.35 BON07
MD
5.63 ± 0.68 BON11
4.22 ± 0.40 BON12
Bonnepierre Gl.
100 meters
10Be sample
Composite moraine distal / proximal side
Moraine crest
Moraine erosion edge
Gully sidewalls
6432000
6431800
961800
962000
962200
962400
d)
0.92 ± 0.14 ETA02
0.91 ± 0.16 ETA01
M1
c. 1410 yrs Rd 62
c. 830 yrs Rd 61
M2
M3: c. AD 1820-1850
AD 1016+ eta01
M4?
Latero-medial moraine
M5: c. AD 1920
c. 530 yrs Rd 60
M6: c. AD 1980
AD 2009
c. 400 yrs Rd 59
c. 680 yrs Rd 57
0 yr Rd 58
Etages Gl.
200 meters
10Be sample
Subfossil log
Delunel et al. (2014a) 10Be glaciogenic sample
6428500
6428000
6427500
957000
957500

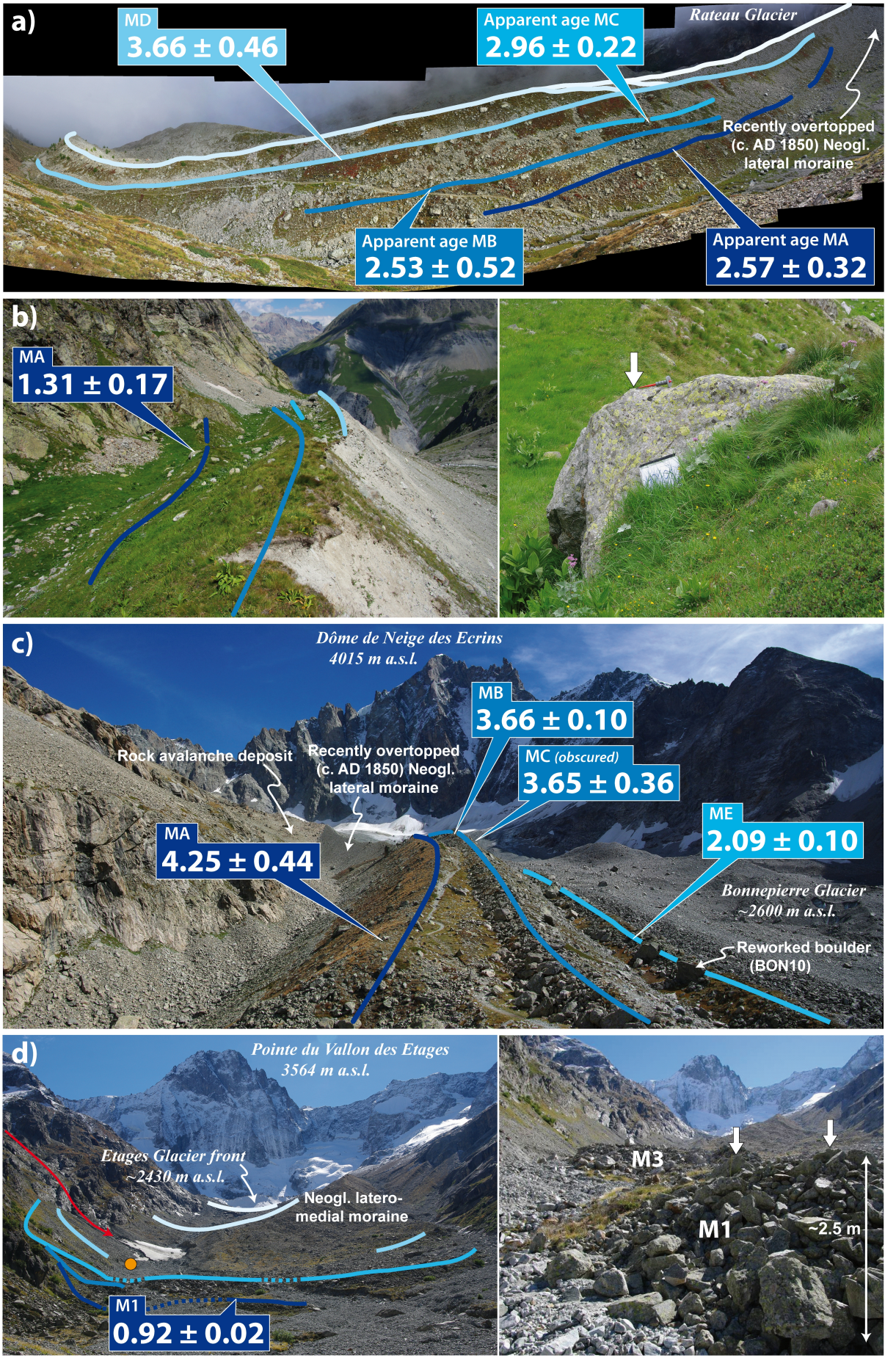
a)
MD
3.66 ± 0.46
Apparent age MC
2.96 ± 0.22
Rateau Glacier
Recently overtopped
(c. AD 1850) Neogl.
lateral moraine
Apparent age MB
2.53 ± 0.52
Apparent age MA
2.57 ± 0.32
b)
MA
1.31 ± 0.17
c)
Dôme de Neige des Ecrins
4015 m a.s.l.
MB
3.66 ± 0.10
Rock avalanche deposit
Recently overtopped
(c. AD 1850) Neogl.
lateral moraine
MC (obscured)
3.65 ± 0.36
ME
2.09 ± 0.10
MA
4.25 ± 0.44
Bonnepierre Glacier
~2600 m a.s.l.
Reworked boulder
(BON10)
d)
Pointe du Vallon des Etages
3564 m a.s.l.
Etages Glacier front
~2430 m a.s.l.
Neogl. latero-
medial moraine
M1
0.92 ± 0.02
M3
M1
~2.5 m

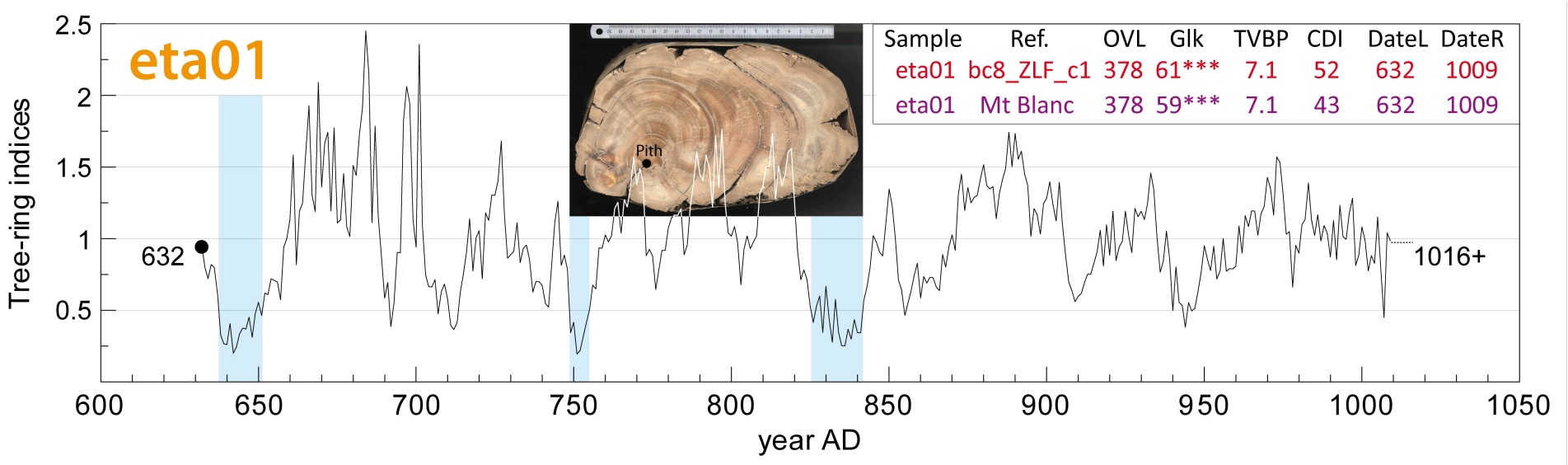
eta01
Pith
Sample Ref. OVL Glk TVBP CDI DateL DateR
eta01 bc8_ZLF_c1 378 61*** 7.1 52 632 1009
eta01 Mt Blanc 378 59*** 7.1 43 632 1009
632
1016+
Tree-ring indices
year AD
2.5
2
1.5
1
0.5
600
650
700
750
800
850
900
950
1000
1050

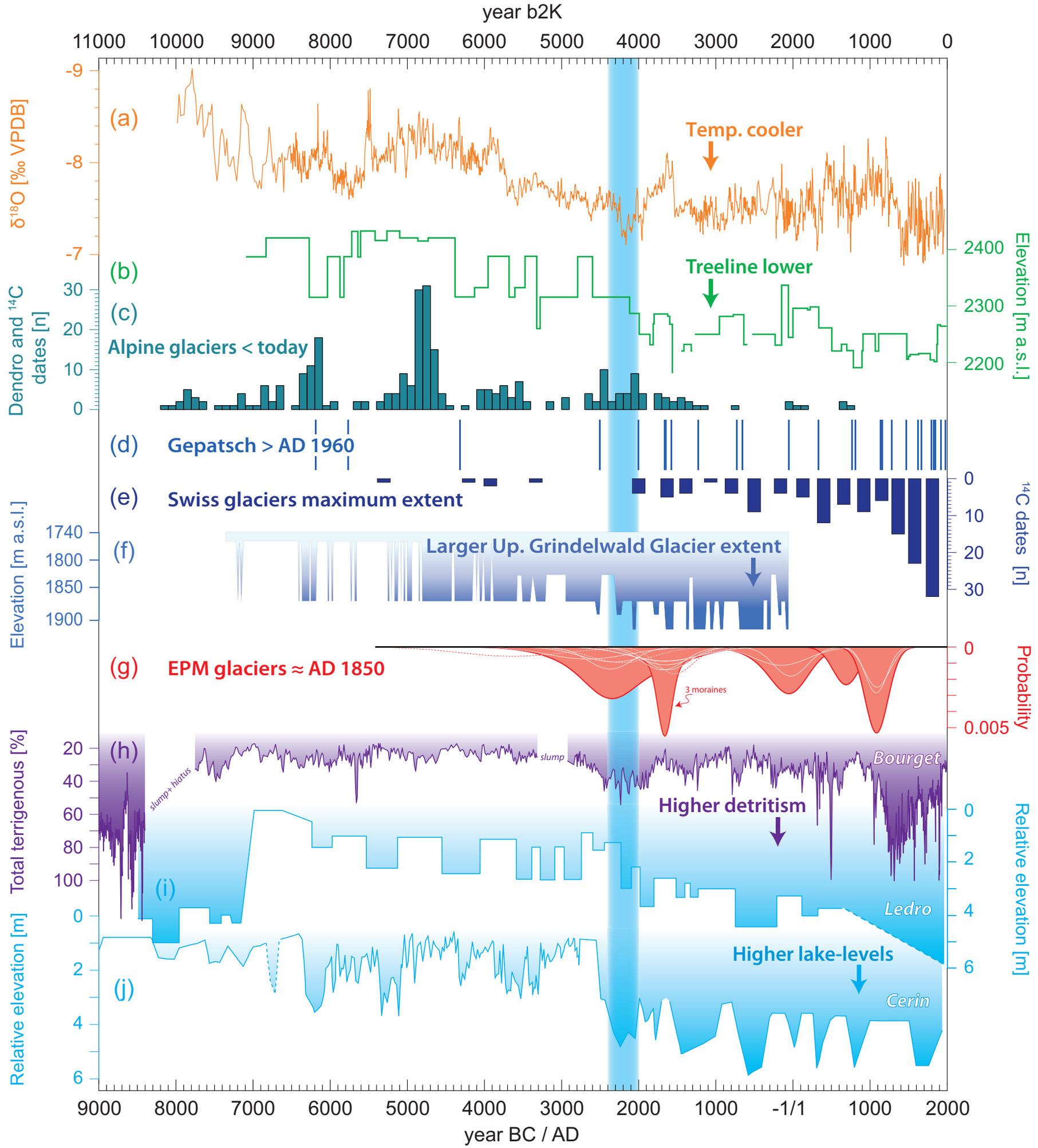
year b2K
11000
10000
9000
8000
7000
6000
5000
4000
3000
2000
1000
0
(a)
δ18O [‰ VPDB]
-9
-8
-7
Temp. cooler
(b)
Treeline lower
Elevation [m a.s.l.]
2400
2300
2200
(c)
Alpine glaciers < today
Dendro and 14C dates [n]
30
20
10
0
(d)
Gepatsch > AD 1960
(e)
Swiss glaciers maximum extent
0
10
20
30
14C dates [n]
(f)
Larger Up. Grindelwald Glacier extent
Elevation [m a.s.l.]
1740
1800
1850
1900
(g)
EPM glaciers ≈ AD 1850
3 moraines
0
0.005
Probability
(h)
slump+ hiatus
slump
Bourget
Higher detritism
Total terrigenous [%]
20
40
60
80
100
(i)
Ledro
Relative elevation [m]
0
2
4
6
Higher lake-levels
(j)
Cerin
Relative elevation [m]
0
2
4
6
9000
8000
7000
6000
5000
4000
3000
2000
1000
-1/1
1000
2000
year BC / AD

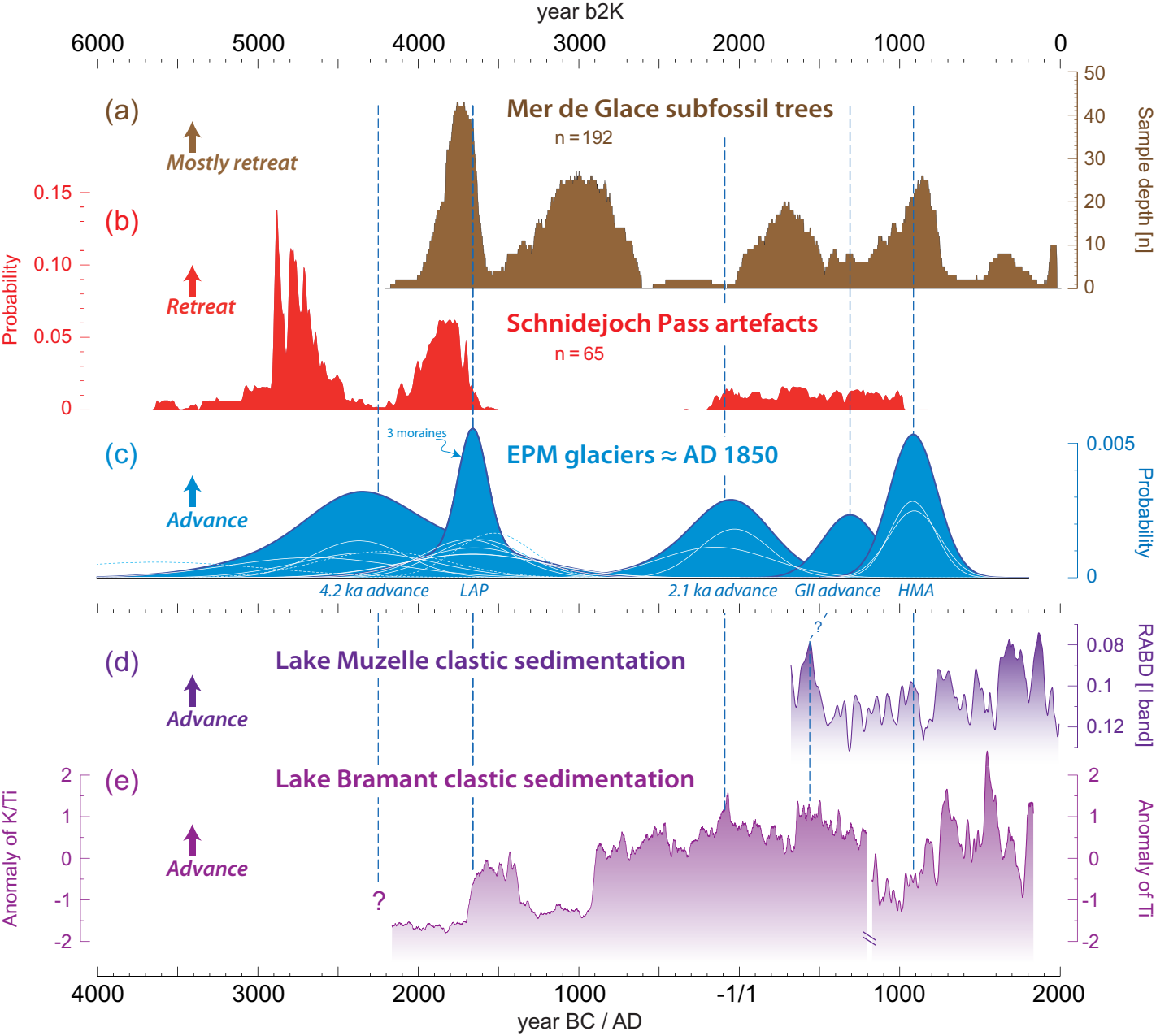
year b2K
6000
5000
4000
3000
2000
1000
0
(a)
Mostly retreat
Mer de Glace subfossil trees
n = 192
Sample depth [n]
50
40
30
20
10
0
(b)
Retreat
Probability
0.15
0.10
0.05
0
Schnidejoch Pass artefacts
n = 65
(c)
3 moraines
EPM glaciers ≈ AD 1850
Advance
0.005
Probability
0
4.2 ka advance
LAP
2.1 ka advance
GII advance
HMA
(d)
Lake Muzelle clastic sedimentation
Advance
?
0.08
0.1
0.12
RABD [I band]
(e)
Lake Bramant clastic sedimentation
Advance
?
Anomaly of K/Ti
2
1
0
-1
-2
Anomaly of Ti
4000
3000
2000
1000
-1/1
1000
2000
year BC / AD

	Neogl. area (km²) [a]	Current area (km²) [b]	Current altitudinal range (m a.s.l.)	Neogl. front (m a.s.l.)	Current average slope (°) [c]	Current aspect (°)	Debris cover (% 2009 area)	MELM	AAR Neogl. ELA (m a.s.l.) [e]	AAR early 1980s ELA (m a.s.l.) [e]	AABR Neogl. ELA (m a.s.l.) [f]	AABR early 1980s ELA (m a.s.l.) [f]
Rateau / Meije	4.83	1.17 (2.95)	3502-2301	1870	34.2	N (13)	28	2760	2651	2834	2761	2914
Lautaret	3.36	0.88 (2.21)	3806-2234	1910	31.0	NE (50)	27 [d]	2540	2737	2832	2847	2932
Bonnepierre	2.62	1.94 (1.97)	3264-2412	2115	20.1	W (287)	54	2880	2862	2876	2792	2816
Etages	3.56	1.12 (1.49)	3224-2431	2095	30.7	N (13)	23	2700	2697	2784	2717	2794
									2737 ± 91	2832 ± 38	2779 ± 55	2864 ± 69
										+ 95 m		+ 85 m

Sample	Latitude (°N)	Longitude (°E)	Elevation (m a.s.l.)	Height above ground (cm) [a]	Lithology	Thickness (cm)	Shielding factor
RAT01	45.018202	6.285005	2399	96	Coarse-grained granite	1.5	0.922
RAT02	45.018125	6.285001	2401	71	Coarse-grained granite	2	0.922
RAT04	45.018282	6.285259	2403	119	Cataclased granite	2.5	0.922
RAT05	45.016606	6.284437	2432	65	Coarse-grained granite	4	0.924
RAT06	45.016990	6.284280	2414	59	Leucocratic gneiss	1.5	0.921
RAT07	45.017344	6.284831	2415	62	Coarse-grained granite	2.5	0.924
RAT08	45.019633	6.286424	2370	70	Coarse-grained granite	2	0.903
RAT09	45.020154	6.286780	2363	115	Massive amphibolite	2.5	0.903
RAT10	45.018670	6.285508	2393	62	Cataclased and chloritised coarse-grained granite	2.5	0.922
LAU01	45.013394	6.350837	2343	110	Fine-grained granite	1.75	0.848
BON00	44.935358	6.325778	2591	230	Aplitic granite	1.75	0.954
BON02	44.935748	6.324149	2581	180	Migmatised gneiss	4	0.955
BON03	44.935888	6.324073	2577	280	Anatectic granite	5	0.955
BON04	44.935833	6.324965	2573	310	Migmatised gneiss	2.5	0.932
BON05	44.935540	6.324488	2584	130	Fine-grained granite	2	0.955
BON06	44.935798	6.323495	2574	150	Fine-grained granite	2.5	0.955
BON07	44.935262	6.325607	2590	110	Migmatised gneiss	2	0.951
BON08	44.936101	6.322237	2553	180	Fine-grained granite	2.5	0.951
BON09	44.936275	6.321760	2545	190	Fine-grained granite	3	0.949
BON10	44.936307	6.321639	2543	190	Migmatised gneiss	2	0.949
BON11	44.935287	6.325250	2587	110	Oriented granite	1.3	0.955
BON12	44.935227	6.325597	2589	85	Anatexic granite	2	0.951
ETA01	44.909085	6.259764	2090	70	Deformed granite	2	0.920
ETA02	44.909090	6.259700	2090	65	Deformed granite	3.5	0.920

Sample	Quartz (g)	Be carrier (mg)	$^{10}Be/^{9}Be$	AMS measured error (%)	$[^{10}Be]$ (at.g^{-1}) [a]	Error (at.g^{-1})	^{10}Be age 'LSD/Chironico' (a) [b]	External uncertainty (a)	^{10}Be age 'Lm/Arctic' (a)	External uncertainty (a)
RAT01	38.3085	0.2897	1.14043E-13	5.1	56800 †	3800	2310	180	2390	190
RAT02	24.3267	0.2953	6.61407E-14	4.6	52100 ‡	3600	2100	160	2200	170
RAT04	29.6413	0.2981	1.09016E-13	5.0	71900 ‡	4900	2970	220	3040	240
RAT05	49.7081	0.2986	1.32735E-13	6.1	52600 †	4100	2100	190	2210	190
RAT06	49.7575	0.2953	1.61997E-13	10.3	63600 †	7300	2580	320	2650	320
RAT07	27.7882	0.3003	1.00990E-13	5.1	71500 ‡	5100	2930	230	2990	240
RAT08	37.3874	0.2893	1.44004E-13	8.9	73600 †	7600	3170	330	3220	350
RAT09	22.4590	0.2924	9.88726E-14	12.4	84500 †	10300	3670	460	3720	480
RAT10	50.5087	0.2963	1.58371E-13	19.5	61400 †	12000	2540	520	2610	520
LAU01	45.9494	0.3005	7.03952E-14	11.0	29600 §	3700	1320	170	1410	180
BON00	45.2676	0.2983	2.41154E-13	11.1	105000 §	12900	3670	450	3750	480
BON02	51.7196	0.2956	3.21659E-13	3.7	122200 †	7400	4380	290	4450	320
BON03	49.6532	0.2993	3.22216E-13	10.1	129100 †	14500	4670	530	4750	560
BON04	36.4583	0.2986	2.18606E-13	8.5	118700 †	11600	4330	430	4400	460
BON05	30.8571	0.2883	1.67223E-13	5.8	103300 †	7600	3630	280	3710	310
BON06	36.1911	0.3148	1.80638E-13	5.0	104000 †	7300	3700	280	3770	300
BON07	16.9800	0.3051	9.66976E-14	8.3	104500 #	9800	3660	360	3760	380
BON08	40.2259	0.2970	1.26189E-13	13.9	60900 §	9200	2160	350	2270	350
BON09	40.0585	0.3028	1.15729E-13	8.6	57100 §	5800	2040	220	2150	230
BON10	44.3182	0.2955	2.21443E-13	4.2	97500 §	6200	3540	240	3630	270
BON11	13.7900	0.3037	1.21111E-13	12.2	164000 #	21800	5640	690	5790	800
BON12	28.0600	0.3023	1.76846E-13	8.9	120300 #	11300	4230	410	4310	440
ETA01	46.9355	0.3017	4.46136E-14	16.7	18400 †	3100	920	160	980	170
ETA02	44.1835	0.3005	4.20809E-14	16.0	18400 †	2800	930	140	980	160